Title

Zn2+ entry through the mitochondrial calcium uniporter is a critical contributor to mitochondrial dysfunction and neurodegeneration.

Authors

Ji, Sung
Medvedeva, Yuliya
Weiss, John

Publication Date

2020-03-01

DOI

10.1016/j.expneurol.2019.113161

Peer reviewed

HHS Public Access

Author manuscript

Exp Neurol. Author manuscript; available in PMC 2020 December 23.

Published in final edited form as:

Exp Neurol. ; 325: 113161. doi:10.1016/j.expneurol.2019.113161.

Zn^{2+} entry through the mitochondrial calcium uniporter is a critical contributor to mitochondrial dysfunction and neurodegeneration

Sung G. Ji[1], **Yuliya V Medvedeva**[2], **John H. Weiss, MD, PhD**[1,2]

[1]Department of Anatomy & Neurobiology, University of California, Irvine

[2]Department of Neurology, University of California, Irvine

Abstract

Excitotoxic Ca^{2+} accumulation contributes to ischemic neurodegeneration, and Ca^{2+} can enter the mitochondria through the mitochondrial calcium uniporter (**MCU**) to promote mitochondrial dysfunction. Yet, Ca^{2+}-targeted therapies have met limited success. A growing body of evidence has highlighted the underappreciated importance of Zn^{2+}, which also accumulates in neurons after ischemia and can induce mitochondrial dysfunction and cell death. While studies have indicated that Zn^{2+} can also enter the mitochondria through the MCU, the specificity of the pore's role in Zn^{2+}-triggered injury is still debated. Present studies use recently available MCU knockout mice to examine how the deletion of this channel impacts deleterious effects of cytosolic Zn^{2+} loading. In cultured cortical neurons from MCU knockout mice, we find significantly reduced mitochondrial Zn^{2+} accumulation. Correspondingly, these neurons were protected from both acute and delayed Zn^{2+}-triggered mitochondrial dysfunction, including mitochondrial reactive oxygen species generation, depolarization, swelling and inhibition of respiration. Furthermore, when toxic extramitochondrial effects of Ca^{2+} entry were moderated, both cultured neurons (exposed to Zn^{2+}) and CA1 neurons of hippocampal slices (subjected to prolonged oxygen glucose deprivation to model ischemia) from MCU knockout mice displayed decreased neurodegeneration. Finally, to examine the therapeutic applicability of these findings, we added an MCU blocker after toxic Zn^{2+} exposure in wildtype neurons (to induce postinsult MCU blockade). This significantly attenuated the delayed evolution of both mitochondrial dysfunction and neurotoxicity. These data—combining both genetic and pharmacologic tools—support the hypothesis that Zn^{2+} entry through the MCU is a critical contributor to ischemic neurodegeneration that could be targeted for neuroprotection.

Address correspondence to: John H. Weiss, MD, Ph.D., 2101 Gillespie Building, Department of Neurology, University of California, Irvine, Irvine, CA 92697-4292, Tel: (949) 824-6774, Fax: (949) 824-1668, jweiss@uci.edu.

Keywords

zinc; calcium; ischemia; excitotoxicity; mitochondria; mitochondrial calcium uniporter; neuronal cultures; hippocampal slice; VSCC; reactive oxygen species; cell death; neurodegeneration; neuroprotection

Introduction

Ischemic stroke is a leading cause of death and disabilities worldwide, with its incidence projected to increase significantly with the aging population (Benjamin et al., 2018). Yet, despite its toll, treatment in humans is limited to attempts at prompt restoration of blood flow, and there are no pharmacologic interventions with demonstrated neuroprotective efficacy. This limitation reflects in part the inability to predict who will suffer from an ischemic event, necessitating a primary focus on treatments delivered after an ischemic event has occurred, and highlights the importance of developing a better understanding of events after an ischemic episode that contribute to delayed neurodegeneration.

A large body of evidence has implicated “excitotoxicity”, caused by excessive release of the excitatory neurotransmitter glutamate, as an important contributor to neuronal injury, and most studies of excitotoxicity have focused on deleterious effects of rapid Ca^{2+} entry through glutamate activated channels (particularly the highly Ca^{2+} permeable N-methyl-D-aspartate [**NMDA**] receptors) (Choi et al., 1988; Rothman and Olney, 1986). Studies of such Ca^{2+}-dependent toxicity indicate the occurrence of multiple injury promoting effects via actions on mitochondria as well as on cytosolic targets (Brennan et al., 2009; Nicholls and Budd, 2000; Siesjo, 1988). Mitochondrial effects of Ca^{2+} appear to result after entry through the mitochondrial Ca^{2+} uniporter (**MCU**). Yet, Ca^{2+} targeting therapies, primarily by blocking Ca^{2+} entry into the cell, have shown little efficacy (Hoyte et al., 2004; Ikonomidou and Turski, 2002). Furthermore, studies using MCU blockers (to block mitochondrial Ca^{2+} uptake) have not only shown mixed results, but also worsened injury in some studies, perhaps in part by preventing mitochondrial buffering of Ca^{2+} loads and resulting in more rapid cytosolic Ca^{2+} loading (Velasco and Tapia, 2000).

Another ion that has been implicated in ischemic neurodegeneration is Zn^{2+}. Zn^{2+} accumulates in neurons after ischemia, primarily from two sources: **1)** Zn^{2+} stored in presynaptic vesicles that can be released with activation (termed “**synaptic Zn^{2+}**”) (Assaf and Chung, 1984; Howell et al., 1984), which can then enter postsynaptic neurons (through voltage-sensitive Ca^{2+} channels [**VSCC**], and with greater rapidity through a subset of AMPA-kainate receptors that are Ca^{2+}-permeable [**Ca-AMPAR**]) (Jia et al., 2002; Kerchner et al., 2000; Weiss et al., 1993; Yin and Weiss, 1995), and **2)** Zn^{2+} already present in postsynaptic neurons which is released from intracellular buffers (primarily metallothionein-III [**MT-III**]) in response to metabolic perturbations associated with ischemia (oxidative stress and acidosis) (Jiang et al., 2000; Maret, 1995). While studies have shown that Zn^{2+} stemming from either one of these sources alone is sufficient to induce injury (Aizenman et al., 2000; Sensi et al., 1999; Weiss et al., 1993), it is apparent that both can synergistically contribute to neuronal injury (Ji and Weiss, 2018), and in fact, the predominant source of Zn^{2+} accumulation contributing to epileptic or ischemic damage appears to differ between

CA1 and CA3 hippocampal pyramidal neurons (Lee et al., 2003; Medvedeva et al., 2017). Prior studies have found Zn^{2+} chelation to be neuroprotective in ischemia (Calderone et al., 2004; Koh et al., 1996), and recent studies of hippocampal slices subjected to oxygen glucose deprivation (**OGD**) as a model of ischemia find that cytosolic Zn^{2+} rises occur early, preceding and contributing to the onset of lethal sharp Ca^{2+} rises (termed "**Ca^{2+} deregulation**") (Medvedeva et al., 2009). Thus, Zn^{2+} may be an attractive target, as its rise occurs before injury becomes irreversible. Interestingly, a critical target of acute deleterious Zn^{2+} effects also appears to be the mitochondria—which Zn^{2+} also enters through the MCU—to potently trigger mitochondrial dysfunction (Clausen et al., 2013; Gazaryan et al., 2007; Ji et al., 2019; Jiang et al., 2001; Malaiyandi et al., 2005; Saris and Niva, 1994). However, past studies elucidating the role of the MCU in Zn^{2+} effects were limited to the use of pharmacologic MCU blockers which lack complete specificity (Tapia and Velasco, 1997). Consequently, one cannot be certain that beneficial effects are specifically due to MCU blockade.

To this end, we took advantage of the recent availability of MCU knockout (**KO**) mice (Pan et al., 2013) and combined this with use of pharmacologic MCU blockers to 1) assess the role of MCU specifically in Zn^{2+}-induced mitochondrial dysfunction and neuronal injury, and 2) examine the ability of delayed MCU blockade (after Zn^{2+} exposures) to attenuate the downstream, deleterious effects of Zn^{2+} on mitochondria. Our findings in both cultured cortical neurons and hippocampal slices provide further support to the hypothesis that Zn^{2+} entry into the mitochondria through the MCU plays a critical role in promoting early and prolonged mitochondrial dysfunction—as well as the consequent neurodegeneration—and that delayed MCU blockade can specifically attenuate these contributions to injury.

Materials and methods

Ethics statement

All procedures for the current study were approved by the Institutional Animal Care and Use Committee of the University of California Irvine, and in accordance with the recommendations from the Guide for the Care and Use of Laboratory Animals of the National Institutes of Health.

Animals

Mice lacking Mitochondrial Calcium Uniporter (Ccdc109a [Mcu], IST11669F8; Texas A&M Institute for Genomic Medicine) were bred from homozygous breeding pairs. Genotype was validated with protocol as detailed previously (Pan et al., 2013), using the following primers: HP3' (CCATCTGTTCCTGACCTTGA), IST11669F8-F (GGAGTTAAGTCATGAGCTGC), and IST11669F8-R (CTGGCTTAGTTGGCAGAGTT). CD-1 mice (used as control and wildtype) were ordered from Charles River (Crl:CD1[ICR]).

Reagents and indicators

Materials for culture maintenance (Minimum Essential Media [**MEM**], fetal bovine serum, glutamine, and horse serum) and for imaging (Newport Green, FluoZin-3 AM, MitoTracker Green, Pluronic F-127, Fura-FF) were purchased from Life Technologies (Grand Island,

NY). Other reagents for experiments (2,2'-dithiodipyridine [**DTDP**], Carbonyl cyanide-p-trifluoromethoxyphenylhydrazone [**FCCP**], Rhodamine 123 [**Rhod123**], Ruthenium Red [**RR**], and N-methyl-D-aspartate [**NMDA**]) were purchased from Sigma-Aldrich (St. Louis, MO). Hydroethidine (**HEt**) was purchased from Assay Biotech (Sunnyvale, CA), MK-801 from Abcam, Apocynin from Acros Organics (Morris Plains, NJ), and XF Base Medium (minimal Dulbecco's Modified Eagle's Medium) from Agilent Technologies (Santa Clara, CA). All other chemicals and reagents were purchased from common commercial sources.

Media

For culture growth and/or maintenance, the following media were used: "Maintenance media" (MEM supplemented with 25 mM glucose), "growth media" (maintenance media supplemented with 10% heatinactivated horse serum 2 mM glutamine), and "plating media" (growth media supplemented with 10% fetal bovine serum). For imaging experiments and/or Zn^{2+} exposures, HEPES-buffered media (consisting of the following [in mM]: 120 NaCl, 5.4 KCl, 0.8 $MgCl_2$, 20 Hepes, 15 glucose, 10 NaOH, in pH 7.4; with either 0 mM $CaCl_2$ [**0 mM Ca^{2+} HSS**] or 1.8 mM $CaCl_2$ [**1.8 mM Ca^{2+} HSS**]) were used, and kept at room temperature unless specified otherwise. To prepare hippocampal slices, isolated brains were maintained in the "preparation solution" (consisting of the following [in mM]: 220 sucrose, 3 KCl, 1.25 NaH_2PO_4, 6 $MgSO_4$, 26 $NaHCO_3$, 0.2 $CaCl_2$, 10 glucose, and 0.42 ketamine, kept in pH 7.35, maintained at 310 mOsm, and equilibrated with 95% O_2/5% CO_2). The hippocampal slices were maintained in artificial cerebral spinal fluid (**ACSF**; consisting of the following [in mM]: 126 NaCl, 3 KCl, 1.25 NaH_2PO_4, 1 $MgSO_4$, 26 $NaHCO_3$, 2 $CaCl_2$, 10 glucose, kept in pH 7.35, maintained at 310 mOsm with sucrose, and equilibrated with 95% O_2/5% CO_2).

Neuronal culture preparation

Mixed cortical neuronal cultures were prepared as described previously (Yin et al., 1994). Briefly, neocortical regions from CD-1 or MCU KO mouse embryos (15 – 16 gestational day; mixed gender) were isolated and cells suspended in plating media. The neuronal suspension was then plated on previously established astrocytic monolayers (of the same genotype) on glass-bottomed dishes, Seahorse XF24 cell culture microplates, or culture-treated 24 well microplates. 2 – 3 days after plating, culture was treated with 10 μM cytosine arabinoside for 24 hrs (to stop non-neuronal cell division), and media was switched to growth media. Cells were kept in 5% CO_2/37°C incubator for at least 10 days prior to experiment. To prepare astrocytic monolayers, the same protocol was used with the following changes: 1) neocortical tissues from postnatal mice (1 – 3 days old; mixed gender) from CD-1 or MCU KO mice were used, 2) plating media was supplemented with epidermal growth factor (10 ng/ml), and 3) suspended cells were plated on poly-D-lysine and laminin-coated glass-bottomed dishes, culture treated 24 well microplates, and Seahorse XF24 cell culture microplates.

Zn^{2+} exposure

Cultured neurons were placed in either 0 mM Ca^{2+} or 1.8 mM Ca^{2+} HSS prior to starting all experiments. After 10 min baseline and pre-treatment with 60 μM DTDP ± 500 μM

Apocynin (if indicated), Zn^{2+} and/or Ca^{2+} loading was induced. To permit ion influx, neurons were exposed to indicated levels of Zn^{2+} (0 – 300 μM) and/or 1.8 mM Ca^{2+} in 90 mM K^+ HSS ("**high K^+**"; HSS modified with 90 mM K^+ and Na^+ adjusted to 35 mM to maintain osmolarity) for 5 min to depolarize neurons, inducing Zn^{2+} and/or Ca^{2+} entry through VSCC. NMDA antagonist MK-801 (10 μM)—used to inhibit Ca^{2+} entry through NMDA receptors—was added during all Zn^{2+} and/or Ca^{2+} exposures (even when Ca^{2+} was not present during the experiment) to maintain consistency. After 5 min Zn^{2+} and/or Ca^{2+} exposure in high K^+, neurons were washed 3 times in HSS (60 μM DTDP ± 500 μM apocynin or 10 μM RR, as indicated). If the experiment involved incubation, cultured neurons were washed 3 times into maintenance media and kept in the 5% CO_2/37°C incubator until needed. When attempting to best model the events that may occur during ischemic conditions, the following standardized paradigm was used when indicated (10 min pre-exposure to 60 μM DTDP, followed by 5 min 100 μM Zn^{2+} + high K^+ + MK-801 + DTDP and 3x wash into DTDP, all in 1.8 mM Ca^{2+} HSS; termed "**ischemic Zn^{2+} exposure**").

Quantitative imaging studies

Neuronal cultures aged 10 – 16 days *in vitro* (**DIV**) were placed on the stage of a Nikon Diaphot inverted microscope equipped with 75 Watts Xenon-lamp, a filter wheel controlled by a computer, a 40x (1.3 numerical aperture) epifluorescence oil-immersion objective along with the following fluorescence cubes: a green FITC (Ex: 480 nm, dichroic: 505 nm, Em: 535 nm) and a red TRITC fluorescence cube (Ex: 540 nm, dichroic: 565 nm, Em: 605 nm). Emitted signals were captured every min with a Sensys Photometrics intensified charge-coupled device camera, and converted digitally by the MetaFluor software (Version 7.0, Molecular Devices LLC, Sunnyvale, CA). Gain and exposure of the camera were adjusted to obtain baseline fluorescence level of 200 – 300 arbitrary units of a 12-bit signal output of 4,096 for all fluorophores. For imaging, only fields with at least 20 healthy looking cells (non-clustered neurons with robust processes) were used. For analysis, background fluorescence (the lowest value in a neuron-free region of the field) was subtracted from images, and fluorescence measurement for each neuron ($\mathbf{F_x}$) was normalized to the average fluorescence intensity of the 10 min baseline measure ($\mathbf{F_0}$) to trend normalized fluorescence over time ($\mathbf{F_x/F_0}$). The F_x/F_0 of each cell in the field was averaged to produce a value constituting one experiment repetition.

Cytosolic Zn^{2+}—Either low affinity cytosolic Zn^{2+} indicator Newport Green diacetate (K_d ~ 1 μM, Ex: 490 nm, Em: 530 nm; using a green FITC fluorescence cube) or the high affinity cytosolic Zn^{2+} indicator FluoZin-3 AM (K_d ~ 15 nM, Ex: 494 nm, Em: 516 nm; using a green FITC fluorescence cube) was used to quantify neuronal Zn^{2+} levels (Canzoniero et al., 1999; Gee et al., 2002; Sensi et al., 1999). Cultured neurons were loaded with 5 μM Newport Green or FluoZin-3 in 0 mM Ca^{2+} HSS containing 0.2% Pluronic F-127 and 1.5% dimethlyl sulfoxide (in the dark room, at room temperature) prior to use for experiments. To assess mitochondrial Zn^{2+} levels, FCCP (1 μM) was added at the end of each experiment to release mitochondrially sequestered Zn^{2+}, with the resulting increase in cytosolic Zn^{2+} level permitting estimate of degree of mitochondrial Zn^{2+} accumulation.

Mitochondrial membrane potential—Mitochondrial membrane potential sensitive indicator Rhod123 (Ex: 507 nm, Em: 529 nm; using a green FITC fluorescence cube) was used to quantify mitochondrial depolarization. Neurons were used for imaging after loading the cultures with 2 μM Rhod123 in 1.8 mM Ca^{2+} HSS for 30 min (in the dark room, at room temperature). Rhod123 is a positively charged dye which accumulates in mitochondria, where its fluorescence is quenched. With mitochondrial depolarization, the Rhod123 sequestered in the mitochondria gets released, resulting in increase in Rhod123 fluorescence intensity (Duchen et al., 2003). FCCP (1 μM; 5 min) was added at the end of each experiment to induce maximal mitochondrial depolarization, permitting measure of maximal Rhod123 ΔF.

Reactive oxygen species—Superoxide sensitive dye HEt (Ex: 510–560 nm; Em: > 590 nm; using a red TRITC fluorescence cube) was used to quantify ROS generation. Neurons were used for imaging after loading the cultures with 5 μM HEt in 0 mM or 1.8 mM Ca^{2+} HSS for 30 min (in the dark room, at room temperature). As HEt is oxidized into highly fluorescent ethidium, ROS generation is quantified as the HEt fluorescence increase.

Mitochondrial respiration assay

Mitochondrial respiration was assessed by measuring changes in O_2 consumption rate (**OCR**) using the Seahorse XF24 Extracellular Flux Analyzer, as described previously with adjustments (Yao et al., 2009). Briefly, neurons plated on top of astrocytic monolayers on Seahorse XF24 Cell Culture Microplates were exposed to the ischemic Zn^{2+} exposure, washed into DTDP for 20 min, and incubated for 2 hrs (in maintenance media and % CO_2/37°C incubator). After completing the incubation, cultures were washed into XF Base Medium (supplemented with 2 mM glutamine, 15 mM glucose, and 1 mM sodium pyruvate), and maintained at 37°C for 1 hr prior to starting the Seahorse XF24 assay. The machine measures the OCR of cells during baseline and after the sequential exposure to 1 μM oligomycin, 2 μM FCCP, and antimycin A/rotenone (both at 1 μM). The concentrations of mitochondrial inhibitors were determined empirically, with FCCP specifically adjusted to induce approximately 1.5x the baseline. Prior to each experiment, all culture wells were visually inspected (to ensure equal distribution of cells) and randomly assigned to treatment groups. All calibration instructions were followed according to the manufacturer's protocols, and Seahorse XF24 program and Wave software were used to run the assay and analyze the data respectively. We carried out prior validation studies confirming astrocytes make minimal contributions to observed OCR and its changes, as our cultured neurons are plated on top of astrocyte monolayers (as discussed above).

Confocal imaging of mitochondrial morphology

Mitochondrial morphology was assessed as described previously (Ji and Weiss, 2018). Briefly, confocal microscopy was performed using an inverted stage Nikon Eclipse Ti chassis microscope with a Yokogawa CSUX spinning disk head. Images were observed at 1000x oil-immersion objective (1.49 numerical aperture) using a Hamamatsu electromultiplying CCD camera. Field was scanned sequentially with excitation (488 nm) via a Coherent sapphire laser source synchronized with the camera, and emission monitored with a 525 (50) nm filter. Images were acquired using the MicroManager Image Acquisition

software (ver 1.52). After cultured neurons were exposed to the ischemic Zn^{2+} exposure paradigm (discussed above) + 20 min wash + 12 hr incubation (in maintenance media at 37°C/5% CO_2), cultures were loaded with 200 nM MitoTracker Green (Ex: 490 nm, Em: 516 nm) in 1.8 mM Ca^{2+} HSS for 30 min at room temperature in the dark, and then switched into 1.8 mM Ca^{2+} HSS for the imaging. Only healthy appearing neurons with intact outer membranes (as could be visualized via brightfield imaging) were chosen for imaging. Camera gain, laser intensity, and exposure times were adjusted to make MitoTracker Green fluorescence intensity 1.5 – 2 times that of the background fluorescence value. Heat fan was used to maintain imaging rig at 37°C. Images acquired were blinded, and lengths and width of distinct mitochondria measured manually in the ImageJ software. The values were used to calculate length/width (**L/W**) ratio of individual mitochondria, which were then averaged to produce one average L/W ratio representing one repetition of an experiment.

Neurotoxicity Assessment

Neurotoxicity was examined in cultured neurons plated on 24 well microplates at 14 – 16 DIV. Briefly, neurons were switched into HSS (0 or 1.8 mM Ca^{2+}), and exposed to 60 μM DTDP (10 min), Zn^{2+} ± Ca^{2+} (in high K^+ and 10 μM MK-801, as discussed above; 5 min) and 10 μM RR (20 min), with concentration as detailed above. After the exposures and treatment, cultures were washed in maintenance media and kept in 37°C/5% CO_2 for 24 hrs, at which cell death was quantified with by lactate dehydrogenase (**LDH**) efflux assay as described (Koh and Choi, 1987). In all experiments, the background LDH present in the media was subtracted by measuring the level in the sham wash protocol, used as negative control, and scaled to levels in positive controls (obtained in cultures exposed to 300 μM NMDA for 24 hrs, a paradigm that reliable destroys >90% of neurons while sparing glia). All wells were visually inspected to estimate degree of cell death, which was compared to quantification from LDH assay, for validation.

Hippocampal slice oxygen-glucose deprivation

Acute hippocampal slices were prepared as described previously (Medvedeva et al., 2009). Briefly, brains from 25 ± 3 days old mice were rapid removed after anesthesia with isoflurane and kept in the ice-cold preparation solution. Hippocampal slices were cut with Leica VT1200 vibratome at 300 μm thickness and placed in ACSF. After slices were equilibrated in ACSF for 1 hr at 34°C, slices were switched into oxygenated ACSF in room temperature for ≥1 hr prior to use.

Slices were mounted on the stage of an upright microscope (BX51WI; Olympus), placed in a flow-through chamber (RC-27L chamber with plastic slice anchor; Warner Instruments), and perfused with the oxygenated ACSF (2 ml/min; 32°C). To measure intracellular Ca^{2+} dynamics, Fura FF (K_d ~ 6 μM) was loaded into individual hippocampal pyramidal neurons using a patch pipette held in the whole cell configuration at – 60 mV for 5 min. After pipette withdrawal, the injected cells were left to recover for 20 min prior to experiment. Fluorescence was alternately excited at 340(20)/380(20) nm via 40× water-immersion objective using a xenon light source (Sutter Instruments) and emitted fluorescence was collected at 532(40) nm using a cooled CCD camera (Hamamatsu). All filters are band pass with bandwidths indicated in parentheses. Images were taken every 15 or 30 s, background

subtracted, and analyzed using the MetaFluor software. Changes in Ca^{2+} levels are displayed as the ratio of background subtracted Fura FF emission intensities upon excitation at 340 and 380 nm ("340/380 ratio").

To model ischemic injury, slices were placed in hypoxic-hypoglycemic condition (via oxygen-glucose deprivation [**OGD**]). ACSF was changed to the same solution lacking glucose (and replaced with sucrose to maintain osmolarity) and bubbled with 95% N_2/5% CO_2. OGD was continued for ≥ 15 min and maintained until Ca^{2+} deregulation occurred.

Statistical analysis

All values on traces are displayed as mean ± standard error of the mean (**SEM**), and on bars displayed as mean + SEM. All experiments were interleaved and have been repeated ≥ 3 times. All comparisons reflect matching sets of cell cultures or slices from the same set of dissections or slice preparation, and all efforts were made to match biologic variables between comparisons. Two-tailed student's t-test was used to assess significance.

Results

Genetic deletion of MCU attenuates mitochondrial Zn^{2+} accumulation in cortical neurons

As prior studies of mitochondrial Zn^{2+} entry through the MCU have only used pharmacologic agents (as discussed above), using the MCU KO mice, we first sought to validate that Zn^{2+} can indeed enter the mitochondria through the MCU, with greater specificity than previously possible. Wildtype (**WT**) and MCU KO cultured neurons were loaded with the low affinity cytosolic Zn^{2+} indicator Newport Green (K_d ~ 1 μM) in 0 mM Ca^{2+} HSS, and exposed to a sequence of 25, 75, and 300 μM exogenous Zn^{2+} (5 min each). Because VSCC are routes of exogenous Zn^{2+} entry through the plasma membrane that are more uniformly expressed across cortical neurons (in contrast to Ca-AMPAR, which are more selectively expressed in specific subsets of neurons), all Zn^{2+} exposures were performed in the presence of 90 mM K^+ ("**high K^+**"; to depolarize neurons, permitting Zn^{2+} influx through VSCC). MK-801 (10 μM), an NMDA receptor blocker used to prevent Ca^{2+} entry, was also added during Zn^{2+} exposures (even in Ca^{2+}-free conditions) in all experiments to eliminate any confounders caused by the channel activation. The dose-response curve consistently displayed greater Newport Green fluorescence rises (**ΔF**)—indicating higher cytosolic Zn^{2+} levels—in MCU KO neurons (Fig 1 top). After the Zn^{2+} exposures, the mitochondrial protonophore, carbonyl cyanide 4-(trifluoromethoxy)phenylhydrazone ("**FCCP**"; 1 μM, 5 min) was added. This dissipates the electrochemical gradient necessary for Zn^{2+} to be retained in mitochondria, leading to release of mitochondrial Zn^{2+} to the cytosol, and the consequent Newport Green ΔF reflects the degree of mitochondrial Zn^{2+} accumulation (Clausen et al., 2013; Ji and Weiss, 2018; Medvedeva et al., 2017; Sensi et al., 2003; Sensi et al., 2002). Note that FCCP increased Newport Green ΔF to similar peak levels in both genotypes, despite MCU KO displaying greater cytosolic Zn^{2+} levels during Zn^{2+} exposures, indicating attenuation of mitochondrial Zn^{2+} accumulation in the MCU KO neurons (Fig 1 top).

After validating Zn^{2+} uptake through the MCU with a spectrum of Zn^{2+} exposures alone, we next examined the role of the pore in permitting Zn^{2+} entry under more physiologic conditions, as may occur during homeostatic Zn^{2+} movement, by inducing partial disruption of endogenous Zn^{2+} buffering and far lower extracellular Zn^{2+} entry. To do so, WT and MCU KO neurons were loaded with high affinity cytosolic Zn^{2+} indicator FluoZin-3 (K_d ~ 15 nM) in 0 mM Ca^{2+} HSS, and exposed to 2,2'-dithiodipyridine (**DTDP**), a thiol oxidant that disrupts Zn^{2+} binding to intracellular buffering proteins, at 60 μM, a concentration which induces partial intracellular Zn^{2+} mobilization (Ji and Weiss, 2018). Neurons were subsequently exposed to 1 μM Zn^{2+} + high K^+ with continued DTDP, followed by wash, and FCCP exposure as indicated (Fig 1 middle). As above, MCU KO neurons displayed significantly greater cytosolic Zn^{2+} levels in response to both intracellular Zn^{2+} mobilization alone as well as the subsequent low Zn^{2+} exposure. Furthermore, the lack of FluoZin-3 ΔF increase in response to FCCP in MCU KO indicates minimal mitochondrial Zn^{2+} accumulation, in contrast to the robust mitochondrial uptake occurring in WT.

While findings thus far support the notion that MCU facilitates mitochondrial Zn^{2+} entry, as Zn^{2+} exposures were carried out in the absence of Ca^{2+}, it is possible that the role MCU plays in Zn^{2+}-triggered mitochondrial dysfunction in pathophysiologic conditions (where Ca^{2+} is present) may be different. To address this, WT and MCU KO neurons were loaded with Newport Green and exposed to DTDP, 100 μM Zn^{2+} + high K^+, wash, and FCCP, all in 1.8 mM Ca^{2+} HSS, as indicated (Fig 1 bottom). This paradigm—combining both disruption of intracellular Zn^{2+} buffering and moderate exogenous Zn^{2+} exposure—was chosen, as it likely best reflects what may occur under pathophysiological conditions like ischemia. Similarly to findings in Ca^{2+}-free conditions, MCU KO neurons still displayed both higher cytosolic Zn^{2+} levels during Zn^{2+} exposure and reduced FCCP-induced mitochondrial Zn^{2+} release, further validating the critical role played by the MCU in permitting mitochondrial Zn^{2+} accumulation, whether from extracellular or intracellular sources.

Zn^{2+}-triggered mitochondrial ROS production is specifically attenuated in MCU KO neurons

We next examined whether Zn^{2+}-triggered ROS production, long considered to be a critical contributor to downstream injury cascades (Ji et al., 2019), is also attenuated in MCU KO neurons. Indeed, as we have previously found that acute Zn^{2+}-induced ROS generation was almost entirely of mitochondrial origin (unlike Ca^{2+}-induced ROS, which had important contributions from both mitochondria and the cytosolic enzyme NADPH oxidase [**NOX**]) (Clausen et al., 2013), we expected minimal Zn^{2+}-triggered ROS generation in MCU KO, corresponding to the attenuated mitochondrial Zn^{2+} accumulation (as shown in Fig 1). Thus, WT and MCU KO neurons were loaded with Hydroethidine (**HEt**; a superoxide sensitive indicator whose fluorescence increase, ΔF, indicates total ROS production) (Bindokas et al., 1996; Clausen et al., 2013; Ji and Weiss, 2018), and exposed to DTDP (60 μM, 10 min), 100 μM Zn^{2+} + high K^+ (5 min), and wash, all in 0 mM Ca^{2+} HSS, as indicated (Fig 2, Top). In contrast to our expectation, there was no difference in HEt ΔF.

This appeared to contradict our prior finding that acute Zn^{2+}-triggered ROS is primarily of mitochondrial origin (Clausen et al., 2013). However, in light of previous studies which

found that prolonged low level Zn^{2+} exposures could induce NOX activity (Noh and Koh, 2000), we hypothesized that the ROS generation in MCU KO could result from NOX upregulation secondary to the impaired mitochondrial Zn^{2+} buffering in the MCU KO, resulting in persistently higher cytosolic Zn^{2+} levels. To test this idea, the experiment was repeated in the presence of the NOX inhibitor, apocynin (500 μM), which almost completely eliminated Zn^{2+}-triggered ROS production in MCU KO neurons while having little effect in WT neurons (Fig 2 Middle). Repeating the experiment in physiological (1.8 mM) Ca^{2+} HSS again revealed near elimination of Zn^{2+}-triggered ROS rise in MCU KO neurons with NOX inhibition (Fig 2 Bottom), further supporting the hypothesis that Zn^{2+}-triggered *mitochondrial* ROS generation is critically dependent upon entry through the MCU.

Critical role of the MCU in acute and delayed Zn^{2+}-triggered mitochondrial dysfunction

We next examined the MCU dependence of other measures of Zn^{2+}-triggered mitochondrial dysfunction. As our goal was to better understand the pore's role in pathophysiologic conditions, we decided to use an exposure paradigm that models events likely to occur in pathological events like ischemia, incorporating both disruption of buffering and uptake of synaptic Zn^{2+} (henceforth termed the "**ischemic Zn^{2+} exposure**"; that parallels the paradigms used in Fig 1 and 2 bottom panels, and comprises 10 min pre-exposure to 60 μM DTDP, followed by 5 min 100 μM Zn^{2+} + high K^+ + DTDP and 3x wash into DTDP, all in 1.8 mM Ca^{2+} HSS; see Materials and methods).

We first examined the role of MCU in Zn^{2+}-triggered loss of mitochondrial membrane potential (**$\Delta\Psi_m$**) using Rhodamine 123 (**Rhod123**; 2 μM), a cationic indicator for which a cytosolic fluorescence increase (**ΔF**) indicates loss of $\Delta\Psi_m$ (see Materials and Methods). WT and MCU KO neurons loaded with Rhod123 were treated to the ischemic Zn^{2+} exposure, washed, and exposed to FCCP as indicated (Fig 3A). The lack of Rhod123 ΔF in MCU KO in response to the Zn^{2+} exposure (compared to the acute ΔF seen after addition of Zn^{2+} in WT neurons), indicates that the Zn^{2+} entry through the MCU is necessary to induce $\Delta\Psi_m$ loss (Fig 3A). FCCP, which causes maximal mitochondrial depolarization, increased Rhod123 ΔF to similar levels in both WT and MCU KO, indicating that the observed difference was not due to differences in the basal $\Delta\Psi_m$ between the two genotypes.

Next, we examined Zn^{2+} effects on mitochondrial energy production using the Seahorse assay, which measures oxygen consumption rate (**OCR**) at baseline and in response to sequential application of mitochondrial inhibitors (oligomycin, FCCP, and antimycin A/rotenone), respectively indicating baseline respiration, ATP-linked respiration, maximum respiratory capacity, and extramitochondrial respiration. WT and MCU KO neurons were treated with either sham or the ischemic Zn^{2+} exposure, washed for 20 min, and incubated for 2 hrs prior to running the assay. Note the substantial preservation of mitochondrial respiration in MCU KO, in contrast to its significant inhibition in WT (Fig 3B).

Finally, we examined the long term effect of Zn^{2+} entry through the MCU on mitochondrial morphology. WT and MCU KO neurons were treated to the ischemic Zn^{2+} exposure, washed for 20 min, and after 12 hr incubation, cultures were loaded with the mitochondrial morphology marker, MitoTracker Green (200 nM) and examined under confocal microscopy (1000x; Fig 3C left). The length and the width of individual mitochondria were then

measured blindly to determine their length/width (**L/W**) ratios, which were then collected to calculate the average L/W ratio of the mitochondria in a single neuron (Fig 3C right). Note that WT neurons showed multiple fragmented, swollen mitochondria (and a corresponding low L/W ratio), while MCU KO mitochondria preserved their morphology, maintaining their elongated structures with high L/W ratio (Fig 3C). These findings, showing significant protection from Zn^{2+}-effects in MCU KO over a spectrum of time, further validate the crucial role of the MCU in the induction of Zn^{2+} triggered mitochondrial dysfunction.

Zn^{2+}-specific contributions to neurotoxicity and ischemic neurodegeneration are attenuated in MCU KO neurons

Next, we sought to determine whether the beneficial effects observed in MCU KO neuronal mitochondria also extend to Zn^{2+}-triggered neurodegeneration. To this aim, WT and MCU KO neurons were subjected to the ischemic Zn^{2+} exposure (labeled as **Ca^{2+} & Zn^{2+}** exposure in Fig 4A), washed for 20 min, and returned to the incubator for 24 hrs prior to assessing cell death. Degree of neurodegeneration was quantified by lactate dehydrogenase (**LDH**) efflux assay and validated by morphological examination (see Materials and methods). To our surprise, in contrast to our findings on mitochondrial dysfunction, both WT and MCU KO neurons displayed similar degrees of neurodegeneration (Fig 4A). In light of prior reports that cells from MCU KO mice were not protected from Ca^{2+}-induced cell death (Nichols et al., 2017; Pan et al., 2013), we next sought to separately assess the Ca^{2+} and Zn^{2+} contributions to neurotoxicity in MCU KO neurons. When neurons were exposed to 1.8 mM Ca^{2+} + high K^+ alone (**Ca^{2+}** only exposure), MCU KO was not protective, and in fact markedly potentiated the Ca^{2+} dependent injury compared to WT neurons. However, with Zn^{2+} + high K^+ (with DTDP) and no Ca^{2+} (**Zn^{2+}** only exposure), MCU KO was protective compared to WT. To determine if MCU KO neurons would display neuroprotection if Ca^{2+} contributions were attenuated, cell death in WT and MCU KO neurons was quantified after the ischemic Zn^{2+} exposure (which includes both Zn^{2+} and Ca^{2+}) was repeated in the presence of the NOX inhibitor apocynin (as in Fig. 2, above), aiming to reduce the injury burden caused by cytosolic Ca^{2+} actions (including Ca^{2+}-induced NOX activation) (Brennan et al., 2009). Indeed, with NOX inhibition, we found significant neuroprotection from Zn^{2+}-induced injury in MCU KO neurons (Fig 4A), supporting the hypothesis that targeting Zn^{2+} entry through the MCU specifically—unlike indiscriminate MCU blockade against both Ca^{2+} and Zn^{2+}—could be neuroprotective.

To test these findings in a model closer to *in vivo* injury, we next examined response to prolonged oxygen-glucose deprivation (**OGD**), as a model of ischemia, in acute hippocampal slices from MCU KO and WT mice. CA1 pyramidal neurons were loaded with low affinity, ratiometric cytosolic Ca^{2+} indicator Fura FF (K_d ~ 6 μM) (Medvedeva et al., 2009; Medvedeva and Weiss, 2014) and subjected to OGD (via perfusion with artificial cerebral spinal fluid [**ACSF**] bubbled with nitrogen gas to remove oxygen, and with glucose replaced by sucrose) with either physiologic (2 mM; Fig 4B left) or low Ca^{2+} levels (200 μM, to minimize Ca^{2+}-contributions to injury; Fig 4B right). Consistent with prior studies using pharmacologic MCU blockade (Medvedeva and Weiss, 2014), MCU KO slices displayed an accelerated onset of the lethal Ca^{2+} deregulation event in response to OGD with physiologic Ca^{2+} (Fig 4B left), possibly reflecting loss the of mitochondrial Ca^{2+}

buffering capacity, and consequent increased cytosolic Ca^{2+} loading and activation of cytosolic Ca^{2+} dependent cell death pathways. However, when Ca^{2+} contributions to injury were attenuated (via lower Ca^{2+} levels), onset of Ca^{2+} deregulation was significantly delayed in MCU KO neurons (Fig 4B right). These data from hippocampal slices show that when extramitochondrial effects of Ca^{2+} are moderated, MCU deletion can confer significant protection against ischemic neurodegeneration. As the degree of this protection is similar to that conferred by Zn^{2+} chelation observed in prior studies (Medvedeva and Weiss, 2014), taken together with our current findings from cultured neurons, these observations support the hypothesis that attenuating mitochondrial Zn^{2+} accumulation through the MCU is neuroprotective.

Delayed MCU blockade attenuates Zn^{2+}-triggered mitochondrial dysfunction and cell death

Finally, to address whether present findings of attenuated Zn^{2+}-triggered injury in MCU KO neurons might be applicable after cellular Zn^{2+} loading has already occurred, we examined the effects of delayed MCU blockade using the pharmacologic agent Ruthenium Red (**RR**). We first assessed changes in rapidly triggered mitochondrial dysfunction. WT neurons, loaded with either Rhod123 (Fig 5A left) or HEt (Fig 5A right), were treated with the ischemic Zn^{2+} exposure and washed into DTDP alone or DTDP + RR (10 μM), followed by FCCP in Rhod123-loaded cultures, as indicated. We found that delayed addition of RR attenuated both loss of $\Delta\Psi_m$ and ROS production even after initial mitochondrial Zn^{2+} loading had already occurred (Fig 5A).

We next set out to determine whether delayed MCU blockade by RR would provide prolonged preservation of mitochondrial morphology. WT neurons were exposed to the same paradigm above (the ischemic Zn^{2+} exposure followed by wash into DTDP ± RR for 20 min) and incubated for 12 hrs, after which mitochondria were labeled with MitoTracker Green and observed under confocal microscopy (as in Fig 3C). Note once again the preservation of elongated mitochondrial structure (corroborated by greater L/W ratio) in neurons treated with RR (Fig 5B). Finally, to test whether delayed MCU blockade could also have neuroprotective effects, the exposure was repeated and cell death assessed after 24 hr incubation (as above). The delayed but transient (20 min) MCU blockade produced a remarkable decrease in neurotoxicity (Fig 5C). These findings show that relatively brief MCU blockade after the insult can dramatically attenuate the downstream events that contribute to neuronal injury.

Discussion

Summary of findings

In the current study, we used the recently available MCU KO mice to evaluate the role of MCU in Zn^{2+}-induced neuronal injury with greater specificity than was previously possible with pharmacological blockers. In cultured cortical neurons, genetic deletion of MCU attenuated mitochondrial Zn^{2+} accumulation, and consequently, diminished its deleterious effects on mitochondria, including loss of $\Delta\Psi_m$, inhibition of respiration, and swelling. While MCU KO surprisingly had little effect on the *total* cellular Zn^{2+}-triggered ROS generation, this appeared to be due to an increased cytosolic NOX activity in the MCU KO

neurons. Indeed, using the NOX antagonist apocynin, we found that *mitochondrial* ROS generation was nearly eliminated in the MCU KO neurons.

In assessing the role of MCU on neurodegeneration 24 hrs after exposures to both Ca^{2+} and Zn^{2+}, we found genetic deletion of MCU was not protective. This death appeared to reflect primarily Ca^{2+} contribution, as further studies revealed accentuation of Ca^{2+}-induced cell death and attenuation of Zn^{2+}-triggered neurodegeneration in the MCU KO neurons. When a NOX antagonist was present during the combined Ca^{2+} and Zn^{2+} exposure, injury in the MCU KO was again significantly attenuated, suggesting that Ca^{2+}-induced activation of upregulated NOX (as mentioned above) was a major contributor to Ca^{2+} triggered neurotoxicity in MCU KO neurons. These findings from cultured neurons were also reflected in the hippocampal slice OGD ischemia model. Whereas MCU KO accelerated OGD-induced cell death of CA1 pyramidal neurons when physiological levels of Ca^{2+} were present, when Ca^{2+} was lowered to abrogate its cytosolic effects, the neurodegeneration in the MCU KO pyramidal neurons was markedly delayed. These findings from the MCU KO cultured neurons and hippocampal slices further strengthen the notion that Zn^{2+} entry through the MCU is a critical contributor to mitochondrial dysfunction and the consequent neurodegeneration.

Finally, as therapeutic interventions in humans will generally entail application of drugs after an ischemic event has occurred, we tested effects of delayed administration of the MCU antagonist, RR, after the Zn^{2+} exposure (again in presence of physiological Ca^{2+}). We found the delayed RR to diminish the induction of acute mitochondrial dysfunction ($\Delta\Psi_m$ and ROS), late mitochondrial swelling, and subsequent cell death, supporting the possible therapeutic utility of delayed targeting of Zn^{2+} entry through the MCU after an ischemic episode has occurred.

Zn^{2+} and ischemic neurodegeneration

As noted above, there is a strong need for greater understanding of injury pathways activated after brief ischemia in order to develop effective interventions. Excitotoxic injury has been strongly implicated in ischemia, and most studies of relevant mechanisms have focused on the critical role of rapid Ca^{2+} entry through NMDA receptors. One target of interest has been mitochondria, which Ca^{2+} enters through the MCU, and with sufficient accumulation, causes a myriad of deleterious effects, including disrupted function, ROS generation, swelling due to opening of mitochondrial permeability transition pore (**mPTP**), and release of Cytochrome C (**CytC**) (Choi et al., 1988; Nicholls and Budd, 2000; Rothman and Olney, 1986). But it has become clear that Ca^{2+} can also induce injury via activation of cytosolic targets, including NOX and catabolic enzymes, with some suggesting that cytosolic Ca^{2+} accumulation may be the key determinant of cell death (Brennan et al., 2009; Murphy et al., 2014; Siesjo, 1988). However, NMDA receptor targeted therapies have shown limited clinical efficacy (Hoyte et al., 2004; Ikonomidou and Turski, 2002). Furthermore, a number of studies finding Zn^{2+} accumulation in injured neurons after ischemia and neuroprotection with Zn^{2+} chelation strongly implicated Zn^{2+} as a contributor to the injury cascade (Calderone et al., 2004; Koh et al., 1996; Tonder et al., 1990; Yin et al., 2002).

An early question concerned the source of Zn^{2+} accumulation. As Zn^{2+} is found in presynaptic vesicles of certain excitatory pathways, from which it can be released with activation (Assaf and Chung, 1984; Frederickson, 1989; Howell et al., 1984; Sloviter, 1985), it was thought that uptake of this synaptic Zn^{2+}—through routes including VSCC and Ca-AMPAR—would account for the accumulation. Yet, studies in ZnT3 KO mice (in which synaptic Zn^{2+} is eliminated due to deletion of the presynaptic vesicular Zn^{2+} transporter, ZnT3) (Cole et al., 1999) found increased Zn^{2+} accumulation in CA1 neurons after prolonged seizures (in contrast to CA3, in which decreased accumulation was noted in the ZnT3 KOs) (Lee et al., 2000; Lee et al., 2003). These findings clearly indicated another source for the Zn^{2+} accumulation, which turned out to be that released from buffering proteins (in particular MT-III) in response to metabolic changes (oxidative stress / acidosis) associated with pathological conditions including ischemia and prolonged seizures (Erickson et al., 1997; Maret, 1995). Indeed, intracellular Zn^{2+} mobilization from this source alone (via the oxidizing agent DTDP) was sufficient to induce both mitochondrial dysfunction and neurotoxicity (Aizenman et al., 2000; Sensi et al., 2003), and it is highly likely that during ischemia, chronic disruption of the intracellular buffering promotes continuous mitochondrial Zn^{2+} influx even after the acute insult (Ji et al., 2019; Medvedeva et al., 2017).

Studies on CA1 and CA3 hippocampal pyramidal neurons (**HPNs**) from transgenic (ZnT3 and MT-III KO) mouse brain slices subjected to OGD provide further support to the idea that the two sources may contribute to their differential vulnerabilities in disease, with CA3 neurons preferentially degenerating after prolonged seizures (Ben-Ari et al., 1980a; Ben-Ari et al., 1980b; Tanaka et al., 1988), and CA1 neurons after transient ischemia (Kirino, 1982; Ordy et al., 1993; Sugawara et al., 1999). In CA3, uptake of synaptic Zn^{2+}, as may occur with repeated neuronal firing during seizures, was the predominant contributor to cytosolic Zn^{2+} accumulation, whereas in CA1, Zn^{2+} release from MT-III predominated, possibly consistent with prolonged metabolic disruption during ischemia causing protracted disruption of intracellular buffering (Medvedeva et al., 2017). Although most studies have examined the 2 sources separately, it is highly likely that they play synergistic roles, and more recent studies on cultured neurons using both exogenous Zn^{2+} exposures *and* DTDP have found even partial disruption of endogenous buffering (via DTDP) to dramatically increase toxic effects of relatively low exogenous Zn^{2+} entry (Ji and Weiss, 2018). Importantly for our current study, this combined exogenous Zn^{2+} and DTDP exposure permits us to more comprehensively model contributions from both Zn^{2+} sources, as likely occurs in ischemia, and when applied to MCU KO neurons, provides important insight into the role of the MCU in Zn^{2+}-contributions to neuronal injury.

Mitochondria: critical, early targets of Zn^{2+} effects

Many studies have identified various targets of Zn^{2+} accumulation that lead to neuronal injury (Kim and Koh, 2002; McLaughlin et al., 2001; Noh and Koh, 2000). However, paralleling Ca^{2+}, early studies suggested Zn^{2+} also has potent effects on mitochondria. Indeed, studies on both isolated mitochondria and cultured neurons have revealed that MCU blockers can also block Zn^{2+} entry into mitochondria, where it appears to induce mitochondrial dysfunction (including loss of $\Delta\Psi_m$, ROS production, mitochondrial swelling,

inhibition of respiration) with far greater potency than Ca^{2+} (Clausen et al., 2013; Gazaryan et al., 2007; Jiang et al., 2001; Saris and Niva, 1994; Sensi et al., 2003), although others have reported a relative paucity of Zn^{2+} effects on mitochondria under conditions where little Ca^{2+} is present (Devinney et al., 2009; Pivovarova et al., 2014). Yet, despite the ability to block both Ca^{2+} and Zn^{2+} uptake into mitochondria, therapeutic attempts using MCU blockers have been disappointing, showing evidence of neuroprotection in some cases, while worsening outcomes in others (Velasco and Tapia, 2000). The reasons for this are not completely clear, but it is possible that by preventing mitochondrial Ca^{2+} uptake, MCU blockade promoted excess cytosolic Ca^{2+} accumulation, leading to loss of cytosolic Ca^{2+} homeostasis that ultimately induced further neuronal injury (Murphy et al., 2014). Furthermore, as the pharmacologic MCU blockers have been characterized to lack full specificity for the MCU and exert numerous nonspecific effects (including VSCC blockade and antioxidant) (Meinicke et al., 1998; Tapia and Velasco, 1997), it was not possible to ascertain whether the effects—protective or not—were indeed specifically due to MCU blockade. In that regard, a key aim of the current study was to model ischemia in *in vitro* culture and slice experiments (via exogenous Zn^{2+} exposure + DTDP and OGD respectively, as discussed above) and use genetic tools to validate and better define the role of the MCU in Zn^{2+} contributions to ischemic neurodegeneration. Our current findings using MCU KO mice not only provide validation that MCU truly is an important route of mitochondrial Zn^{2+} entry that promotes mitochondrial dysfunction, but also reveals that targeting Zn^{2+} specifically through the MCU—rather than indiscriminate MCU blockade, which can actually exacerbate Ca^{2+}-triggered injury—can provide significant neuroprotection. Indeed, the recent identification of the MCU gene and its associated regulatory peptides (De Stefani et al., 2015; Kamer and Mootha, 2015; Marchi and Pinton, 2014) provided a major opportunity for breakthrough in the study of these channels. Interestingly, the regulatory subunits MICU1 and 2 appear to respond to Ca^{2+} to enable pore opening, preventing pore opening when Ca^{2+} is low and opening it when Ca^{2+} rises – conferring a sigmoid shaped Ca^{2+} concentration, channel activation relationship. These findings may have implications for Zn^{2+} effects on mitochondria as well, especially in light of prior evidence that Ca^{2+} not only is necessary for Zn^{2+} effects in certain conditions (as discussed above), but also enhances Zn^{2+} entry through the MCU (Saris and Niva, 1994). Furthermore, we and others have observed evidence for synergism between Zn^{2+} and Ca^{2+} on mitochondria, with far greater effects of Zn^{2+} in presence of Ca^{2+} (Gazaryan et al., 2007; Ji and Weiss, 2018; Jiang et al., 2001; Sensi et al., 2000), which could be explained in part by Ca^{2+} dependence of the MCU pore opening.

Delayed targeting of Zn^{2+} for protection against ischemia

Studies in hippocampal slice OGD models of ischemia have yielded important clues to how Zn^{2+} may contribute to ischemic neurodegeneration. Early studies clearly showed acute extracellular and intracellular Zn^{2+} rises (Li et al., 2001; Wei et al., 2004), but interactions between Zn^{2+} and Ca^{2+} effects were unexplored. Thus, we carried out the first study monitoring Ca^{2+} and Zn^{2+} simultaneously in single CA1 HPNs, and found Zn^{2+} rises to precede and contribute to lethal Ca^{2+} deregulation. Furthermore, this seemed to depend upon Zn^{2+} uptake into mitochondria (Medvedeva et al., 2009). To test the relevance of these findings, we carried out *in vivo* global ischemia studies in rats, where after inducing

transient cardiac arrest, we used the Timm's sulfide silver stain to label reactive Zn^{2+}, and observed neurons under electron microscopy to examine both subcellular localization of Zn^{2+} and mitochondrial morphology (Yin et al., 2019). We found evidence of delayed and progressive mitochondrial Zn^{2+} accumulation in CA1 neurons, with the degree of accumulation correlating with the extent of mitochondrial structural disruption. These findings in hippocampal slices and whole animal models further support a critical role of mitochondrial Zn^{2+} accumulation as an early factor in ischemic neurodegeneration the targeting of which may yield protection.

To test the role of MCU in this injury cascade, pharmacologic blockers (RR or the more specific analogue Ru-360) were added prior to prolonged OGD in hippocampal slices, which surprisingly accelerated the lethal Ca^{2+} deregulation. As this may have been due to MCU blockers hastening cytosolic Ca^{2+} accumulation by inhibiting mitochondrial Ca^{2+} uptake, the experiment was repeated with ACSF Ca^{2+} lowered from 2 mM to 200 μM; under these circumstances, the blocker became highly protective. Additional findings that (in low Ca^{2+} conditions) the degree of protection from MCU blockade was similar to that from Zn^{2+} chelation supported the idea that the protection from MCU blockers was due to antagonism of Zn^{2+} entry into mitochondria via the MCU (Medvedeva and Weiss, 2014). Present studies using the MCU KO slice model subjected to prolonged OGD further validate these prior results, supporting the idea that attenuating Zn^{2+} entry specifically through MCU can provide neuroprotection. Yet, as these studies entailed either pretreatment with MCU blocker or genetic knockout, they are limited in utility for translation. Indeed, attenuating MCU activity prior to insult appears to exacerbate peak Ca^{2+} loading and worsens Ca^{2+} dependent injury, and as ischemic events cannot be predicted in patients, most opportunities for intervention are after the acute ischemic insult. Furthermore, given the profound protective effects of attenuating Zn^{2+} entry found in the MCU KO mice, delayed interventions targeting the MCU may be particularly beneficial, as it would reduce Zn^{2+} influx into mitochondria that likely continues to occur after ischemic insult.

To address mechanisms of such delayed injury after transient ischemia, we subjected slices to sublethal episodes of OGD (in which OGD was aborted shortly prior to the expected time of Ca^{2+} deregulation). We found that mitochondrial Zn^{2+} entry was an early event in response to sublethal OGD in both CA1 and CA3 regions. However, CA1 neurons had prolonged (> 1hr) Zn^{2+} accumulation in mitochondria that progressed during the period after OGD, and which appeared to contribute to delayed mitochondrial swelling. In contrast, far less late mitochondrial Zn^{2+} accumulation was observed in the CA3 neurons. Given the particular vulnerability of CA1 neurons to delayed ischemic degeneration, it is possible that this early mitochondrial Zn^{2+} accumulation and prolonged sequestration is a key trigger of the persistent mitochondrial dysfunction, including mitochondrial swelling, CytC release and mitochondrial multi-conductance channel activation observed in some animal studies (Bonanni et al., 2006; Calderone et al., 2004; Sugawara et al., 1999). Late administration of the MCU blocker RR diminished both the delayed Zn^{2+} accumulation within the mitochondria and the consequent mitochondrial swelling 1 hr after sublethal OGD in CA1 HPNs (Medvedeva et al., 2017).

Present findings of protective effects of late RR after Zn^{2+} exposures to cultured WT cortical neurons are consistent with prior studies, providing further support to the idea that delayed mitochondrial Zn^{2+} accumulation contributes to mitochondrial dysfunction and delayed neurodegeneration and supports the utility of late interventions. Indeed, by permitting buffering of acute cytosolic Ca^{2+} loads by the mitochondria prior to MCU blockade, late administration of these antagonists after the insult may abrogate the problem of enhanced cytosolic Ca^{2+} loading seen with pretreatment. Although the available antagonists lack full specificity for this channel and their other actions (including antioxidant effects) could theoretically contribute to their benefit, we found that application of RR did not significantly attenuate Zn^{2+}-triggered ROS production in MCU KO neurons (data not shown), suggesting the benefits in RR treated WT neurons were indeed due to MCU blockade rather than nonspecific effects. Combined with present findings using the MCU KO, our data on delayed MCU blockade provide compelling support to the notion that post-injury antagonism of mitochondrial Zn^{2+} accumulation could play a crucial role as a future neuroprotective strategy.

Conclusions

In summary, present findings lend new support to the hypothesis that the MCU plays a critical role in Zn^{2+}-triggered mitochondrial dysfunction and the subsequent neurotoxicity. Furthermore, the strong protection provided by delayed MCU blockade may lend further new support to the potential utility of delayed MCU blockade to attenuate mitochondrial Zn^{2+} accumulation even after ischemia.

Based on these observations, we propose the following model during ischemia: 1) Zn^{2+} accumulates in the cytosol due to combination of synaptic Zn^{2+} uptake and release from buffers, 2) accumulated Zn^{2+} enters the mitochondria via the MCU, with the degree of mitochondrial dysfunction reflecting combination of both the amount and the duration of mitochondrial Zn^{2+} loading. 3) In lethal ischemia, overwhelming mitochondrial Zn^{2+} accumulation occurs during ischemic insult to cause mitochondrial failure and promote acute lethal cytosolic Ca^{2+} overload, ultimately leading to rapid cell death. 4) If ischemic episode is transient, the mitochondria may have already depolarized sufficiently to release much of their accumulated Zn^{2+}, but during recovery, they begin to repolarize and Zn^{2+} re-accumulates into the mitochondria. 5) This re-accumulation promotes more mitochondrial ROS generation, and aided by the post-injury oxidative environment (which can continue disrupting intracellular Zn^{2+} buffering to create a feed forward cascade of mitochondrial Zn^{2+} loading), lead to more mitochondrial dysfunction. 6) The accompanying consequences, including mPTP opening, CytC release, and irreversible oxidative damage, may be critical upstream events in triggering delayed degeneration pathways. Thus, targeting of either the early mitochondrial Zn^{2+} accumulation and/or the delayed Zn^{2+} re-accumulation into the mitochondria—both through the MCU—may yield significant benefit by impeding activation of these delayed injury pathways.

Acknowledgements

Supported by NIH grants NS096987 and NS100494 (JHW), and the American Heart Association grants 17GRNT33410181 (JHW) and 16PRE29560003 (SGJ). The authors declare no competing financial interests.

Abbreviations

Ca-AMPAR	Ca^{2+} permeable AMPA receptors
FCCP	carbonyl cyanide-p-trifluoromethoxyphenylhydrazone
DTDP	2,2'-dithiodipyridine
HEt	hydroethidine
KO	knockout
MT	metallothionein
MCU	mitochondrial calcium uniporter
NMDA	N-methyl-D-aspartate
OGD	oxygen glucose deprivation
ROS	reactive oxygen species
Rhod123	rhodamine 123
VSCC	voltage sensitive Ca^{2+} channels

References

Aizenman E, Stout AK, Hartnett KA, Dineley KE, McLaughlin B, Reynolds IJ, 2000 Induction of neuronal apoptosis by thiol oxidation: putative role of intracellular zinc release. J Neurochem 75, 1878–1888. [PubMed: 11032877]

Assaf SY, Chung SH, 1984 Release of endogenous Zn2+ from brain tissue during activity. Nature 308, 734–736. [PubMed: 6717566]

Ben-Ari Y, Tremblay E, Ottersen OP, 1980a Injections of kainic acid into the amygdaloid complex of the rat: an electrographic, clinical and histological study in relation to the pathology of epilepsy. Neuroscience 5, 515–528. [PubMed: 6892841]

Ben-Ari Y, Tremblay E, Ottersen OP, Meldrum BS, 1980b The role of epileptic activity in hippocampal and "remote" cerebral lesions induced by kainic acid. Brain research 191, 79–97. [PubMed: 7378761]

Benjamin EJ, Virani SS, Callaway CW, Chamberlain AM, Chang AR, Cheng S, Chiuve SE, Cushman M, Delling FN, Deo R, de Ferranti SD, Ferguson JF, Fornage M, Gillespie C, Isasi CR, Jimenez MC, Jordan LC, Judd SE, Lackland D, Lichtman JH, Lisabeth L, Liu S, Longenecker CT, Lutsey PL, Mackey JS, Matchar DB, Matsushita K, Mussolino ME, Nasir K, O'Flaherty M, Palaniappan LP, Pandey A, Pandey DK, Reeves MJ, Ritchey MD, Rodriguez CJ, Roth GA, Rosamond WD, Sampson UKA, Satou GM, Shah SH, Spartano NL, Tirschwell DL, Tsao CW, Voeks JH, Willey JZ, Wilkins JT, Wu JH, Alger HM, Wong SS, Muntner P, American Heart Association Council on, E., Prevention Statistics, C., Stroke Statistics, S., 2018 Heart Disease and Stroke Statistics-2018 Update: A Report From the American Heart Association. Circulation 137, e67–e492. [PubMed: 29386200]

Bindokas VP, Jordan J, Lee CC, Miller RJ, 1996 Superoxide production in rat hippocampal neurons: selective imaging with hydroethidine. J Neurosci 16, 1324–1336. [PubMed: 8778284]

Bonanni L, Chachar M, Jover-Mengual T, Li H, Jones A, Yokota H, Ofengeim D, Flannery RJ, Miyawaki T, Cho CH, Polster BM, Pypaert M, Hardwick JM, Sensi SL, Zukin RS, Jonas EA, 2006 Zinc-dependent multi-conductance channel activity in mitochondria isolated from ischemic brain. J Neurosci 26, 6851–6862. [PubMed: 16793892]

Brennan AM, Suh SW, Won SJ, Narasimhan P, Kauppinen TM, Lee H, Edling Y, Chan PH, Swanson RA, 2009 NADPH oxidase is the primary source of superoxide induced by NMDA receptor activation. Nature neuroscience 12, 857–863. [PubMed: 19503084]

Calderone A, Jover T, Mashiko T, Noh KM, Tanaka H, Bennett MV, Zukin RS, 2004 Late calcium EDTA rescues hippocampal CA1 neurons from global ischemia-induced death. J Neurosci 24, 9903–9913. [PubMed: 15525775]

Canzoniero LM, Turetsky DM, Choi DW, 1999 Measurement of intracellular free zinc concentrations accompanying zinc-induced neuronal death. J Neurosci 19, RC31. [PubMed: 10493776]

Choi DW, Koh JY, Peters S, 1988 Pharmacology of glutamate neurotoxicity in cortical cell culture: attenuation by NMDA antagonists. J Neurosci 8, 185–196. [PubMed: 2892896]

Clausen A, McClanahan T, Ji SG, Weiss JH, 2013 Mechanisms of Rapid Reactive Oxygen Species Generation in response to Cytosolic Ca2+ or Zn2+ Loads in Cortical Neurons. Plos One 8, e83347. [PubMed: 24340096]

Cole TB, Wenzel HJ, Kafer KE, Schwartzkroin PA, Palmiter RD, 1999 Elimination of zinc from synaptic vesicles in the intact mouse brain by disruption of the ZnT3 gene. Proc Natl Acad Sci U S A 96, 1716–1721. [PubMed: 9990090]

De Stefani D, Patron M, Rizzuto R, 2015 Structure and function of the mitochondrial calcium uniporter complex. Biochim Biophys Acta 1853, 2006–2011. [PubMed: 25896525]

Devinney MJ, Malaiyandi LM, Vergun O, DeFranco DB, Hastings TG, Dineley KE, 2009 A comparison of Zn2+- and Ca2+-triggered depolarization of liver mitochondria reveals no evidence of Zn2+-induced permeability transition. Cell Calcium 45, 447–455. [PubMed: 19349076]

Duchen MR, Surin A, Jacobson J, 2003 Imaging mitochondrial function in intact cells. Methods Enzymol 361, 353–389. [PubMed: 12624920]

Erickson JC, Hollopeter G, Thomas SA, Froelick GJ, Palmiter RD, 1997 Disruption of the metallothionein-III gene in mice: analysis of brain zinc, behavior, and neuron vulnerability to metals, aging, and seizures. J Neurosci 17, 1271–1281. [PubMed: 9006971]

Frederickson CJ, 1989 Neurobiology of zinc and zinc-containing neurons. Int Rev Neurobiol 31, 145–238. [PubMed: 2689380]

Gazaryan IG, Krasinskaya IP, Kristal BS, Brown AM, 2007 Zinc irreversibly damages major enzymes of energy production and antioxidant defense prior to mitochondrial permeability transition. J Biol Chem 282, 24373–24380. [PubMed: 17565998]

Gee KR, Zhou ZL, Ton-That D, Sensi SL, Weiss JH, 2002 Measuring zinc in living cells. A new generation of sensitive and selective fluorescent probes. Cell calcium 31, 245–251. [PubMed: 12098227]

Howell GA, Welch MG, Frederickson CJ, 1984 Stimulation-induced uptake and release of zinc in hippocampal slices. Nature 308, 736–738. [PubMed: 6717567]

Hoyte L, Barber PA, Buchan AM, Hill MD, 2004 The rise and fall of NMDA antagonists for ischemic stroke. Current molecular medicine 4, 131–136. [PubMed: 15032709]

Ikonomidou C, Turski L, 2002 Why did NMDA receptor antagonists fail clinical trials for stroke and traumatic brain injury? The Lancet. Neurology 1, 383–386. [PubMed: 12849400]

Ji SG, Medvedeva YV, Wang HL, Yin HZ, Weiss JH, 2019 Mitochondrial Zn(2+) Accumulation: A Potential Trigger of Hippocampal Ischemic Injury. The Neuroscientist : a review journal bringing neurobiology, neurology and psychiatry 25, 126–138.

Ji SG, Weiss JH, 2018 Zn(2+)-induced disruption of neuronal mitochondrial function: Synergism with Ca(2+), critical dependence upon cytosolic Zn(2+) buffering, and contributions to neuronal injury. Exp Neurol 302, 181–195. [PubMed: 29355498]

Jia Y, Jeng JM, Sensi SL, Weiss JH, 2002 Zn2+ currents are mediated by calcium-permeable AMPA/kainate channels in cultured murine hippocampal neurones. The Journal of physiology 543, 35–48. [PubMed: 12181280]

Jiang D, Sullivan PG, Sensi SL, Steward O, Weiss JH, 2001 Zn(2+) induces permeability transition pore opening and release of pro-apoptotic peptides from neuronal mitochondria. J Biol Chem 276, 47524–47529. [PubMed: 11595748]

Jiang LJ, Vasak M, Vallee BL, Maret W, 2000 Zinc transfer potentials of the alpha - and beta-clusters of metallothionein are affected by domain interactions in the whole molecule. Proc Natl Acad Sci U S A 97, 2503–2508. [PubMed: 10716985]

Kamer KJ, Mootha VK, 2015 The molecular era of the mitochondrial calcium uniporter. Nature reviews. Molecular cell biology 16, 545–553. [PubMed: 26285678]

Kerchner GA, Canzoniero LM, Yu SP, Ling C, Choi DW, 2000 Zn2+ current is mediated by voltage-gated Ca2+ channels and enhanced by extracellular acidity in mouse cortical neurones. The Journal of physiology 528 Pt 1, 39–52. [PubMed: 11018104]

Kim YH, Koh JY, 2002 The role of NADPH oxidase and neuronal nitric oxide synthase in zinc-induced poly(ADP-ribose) polymerase activation and cell death in cortical culture. Experimental neurology 177, 407–418. [PubMed: 12429187]

Kirino T, 1982 Delayed neuronal death in the gerbil hippocampus following ischemia. Brain research 239, 57–69. [PubMed: 7093691]

Koh JY, Choi DW, 1987 Quantitative determination of glutamate mediated cortical neuronal injury in cell culture by lactate dehydrogenase efflux assay. Journal of neuroscience methods 20, 83–90. [PubMed: 2884353]

Koh JY, Suh SW, Gwag BJ, He YY, Hsu CY, Choi DW, 1996 The role of zinc in selective neuronal death after transient global cerebral ischemia. Science 272, 1013–1016. [PubMed: 8638123]

Lee JY, Cole TB, Palmiter RD, Koh JY, 2000 Accumulation of zinc in degenerating hippocampal neurons of ZnT3-null mice after seizures: evidence against synaptic vesicle origin. J Neurosci 20, RC79. [PubMed: 10807937]

Lee JY, Kim JH, Palmiter RD, Koh JY, 2003 Zinc released from metallothionein-iii may contribute to hippocampal CA1 and thalamic neuronal death following acute brain injury. Exp Neurol 184, 337–347. [PubMed: 14637104]

Li Y, Hough CJ, Suh SW, Sarvey JM, Frederickson CJ, 2001 Rapid translocation of Zn(2+) from presynaptic terminals into postsynaptic hippocampal neurons after physiological stimulation. Journal of neurophysiology 86, 2597–2604. [PubMed: 11698545]

Malaiyandi LM, Vergun O, Dineley KE, Reynolds IJ, 2005 Direct visualization of mitochondrial zinc accumulation reveals uniporter-dependent and -independent transport mechanisms. J Neurochem 93, 1242–1250. [PubMed: 15934944]

Marchi S, Pinton P, 2014 The mitochondrial calcium uniporter complex: molecular components, structure and physiopathological implications. The Journal of physiology 592, 829–839. [PubMed: 24366263]

Maret W, 1995 Metallothionein/disulfide interactions, oxidative stress, and the mobilization of cellular zinc. Neurochemistry international 27, 111–117. [PubMed: 7655343]

McLaughlin B, Pal S, Tran MP, Parsons AA, Barone FC, Erhardt JA, Aizenman E, 2001 p38 activation is required upstream of potassium current enhancement and caspase cleavage in thiol oxidant-induced neuronal apoptosis. J Neurosci 21, 3303–3311. [PubMed: 11331359]

Medvedeva YV, Ji SG, Yin HZ, Weiss JH, 2017 Differential Vulnerability of CA1 versus CA3 Pyramidal Neurons After Ischemia: Possible Relationship to Sources of Zn2+ Accumulation and Its Entry into and Prolonged Effects on Mitochondria. J Neurosci 37, 726–737. [PubMed: 28100752]

Medvedeva YV, Lin B, Shuttleworth CW, Weiss JH, 2009 Intracellular Zn2+ accumulation contributes to synaptic failure, mitochondrial depolarization, and cell death in an acute slice oxygen-glucose deprivation model of ischemia. J Neurosci 29, 1105–1114. [PubMed: 19176819]

Medvedeva YV, Weiss JH, 2014 Intramitochondrial Zn(2+) accumulation via the Ca(2+) uniporter contributes to acute ischemic neurodegeneration. Neurobiol Dis 68, 137–144. [PubMed: 24787898]

Meinicke AR, Bechara EJ, Vercesi AE, 1998 Ruthenium red-catalyzed degradation of peroxides can prevent mitochondrial oxidative damage induced by either tert-butyl hydroperoxide or inorganic phosphate. Archives of biochemistry and biophysics 349, 275–280. [PubMed: 9448715]

Murphy E, Pan X, Nguyen T, Liu J, Holmstrom KM, Finkel T, 2014 Unresolved questions from the analysis of mice lacking MCU expression. Biochemical and biophysical research communications 449, 384–385. [PubMed: 24792186]

Nicholls DG, Budd SL, 2000 Mitochondria and neuronal survival. Physiol Rev 80, 315–360. [PubMed: 10617771]

Nichols M, Elustondo PA, Warford J, Thirumaran A, Pavlov EV, Robertson GS, 2017 Global ablation of the mitochondrial calcium uniporter increases glycolysis in cortical neurons subjected to energetic stressors. Journal of cerebral blood flow and metabolism : official journal of the International Society of Cerebral Blood Flow and Metabolism 37, 3027–3041.

Noh KM, Koh JY, 2000 Induction and activation by zinc of NADPH oxidase in cultured cortical neurons and astrocytes. J Neurosci 20, RC111. [PubMed: 11090611]

Ordy JM, Wengenack TM, Bialobok P, Coleman PD, Rodier P, Baggs RB, Dunlap WP, Kates B, 1993 Selective vulnerability and early progression of hippocampal CA1 pyramidal cell degeneration and GFAP-positive astrocyte reactivity in the rat four-vessel occlusion model of transient global ischemia. Experimental neurology 119, 128–139. [PubMed: 8432346]

Pan X, Liu J, Nguyen T, Liu C, Sun J, Teng Y, Fergusson MM, Rovira II, Allen M, Springer DA, Aponte AM, Gucek M, Balaban RS, Murphy E, Finkel T, 2013 The physiological role of mitochondrial calcium revealed by mice lacking the mitochondrial calcium uniporter. Nature cell biology 15, 1464–1472. [PubMed: 24212091]

Pivovarova NB, Stanika RI, Kazanina G, Villanueva I, Andrews SB, 2014 The interactive roles of zinc and calcium in mitochondrial dysfunction and neurodegeneration. J Neurochem 128, 592–602. [PubMed: 24127746]

Rothman SM, Olney JW, 1986 Glutamate and the pathophysiology of hypoxic--ischemic brain damage. Ann Neurol 19, 105–111. [PubMed: 2421636]

Saris NE, Niva K, 1994 Is Zn2+ transported by the mitochondrial calcium uniporter? FEBS Lett 356, 195–198. [PubMed: 7528685]

Sensi SL, Ton-That D, Sullivan PG, Jonas EA, Gee KR, Kaczmarek LK, Weiss JH, 2003 Modulation of mitochondrial function by endogenous Zn2+ pools. Proc Natl Acad Sci U S A 100, 6157–6162. [PubMed: 12724524]

Sensi SL, Ton-That D, Weiss JH, 2002 Mitochondrial sequestration and Ca(2+)-dependent release of cytosolic Zn(2+) loads in cortical neurons. Neurobiology of disease 10, 100–108. [PubMed: 12127148]

Sensi SL, Yin HZ, Carriedo SG, Rao SS, Weiss JH, 1999 Preferential Zn2+ influx through Ca2+-permeable AMPA/kainate channels triggers prolonged mitochondrial superoxide production. Proc Natl Acad Sci U S A 96, 2414–2419. [PubMed: 10051656]

Sensi SL, Yin HZ, Weiss JH, 2000 AMPA/kainate receptor-triggered Zn2+ entry into cortical neurons induces mitochondrial Zn2+ uptake and persistent mitochondrial dysfunction. The European journal of neuroscience 12, 3813–3818. [PubMed: 11029652]

Siesjo BK, 1988 Historical overview. Calcium, ischemia, and death of brain cells. Annals of the New York Academy of Sciences 522, 638–661. [PubMed: 2454060]

Sloviter RS, 1985 A selective loss of hippocampal mossy fiber Timm stain accompanies granule cell seizure activity induced by perforant path stimulation. Brain research 330, 150–153. [PubMed: 2859083]

Sugawara T, Fujimura M, Morita-Fujimura Y, Kawase M, Chan PH, 1999 Mitochondrial release of cytochrome c corresponds to the selective vulnerability of hippocampal CA1 neurons in rats after transient global cerebral ischemia. J Neurosci 19, RC39. [PubMed: 10559429]

Tanaka S, Kondo S, Tanaka T, Yonemasu Y, 1988 Long-term observation of rats after unilateral intra-amygdaloid injection of kainic acid. Brain research 463, 163–167. [PubMed: 3196905]

Tapia R, Velasco I, 1997 Ruthenium red as a tool to study calcium channels, neuronal death and the function of neural pathways. Neurochemistry international 30, 137–147. [PubMed: 9017661]

Tonder N, Johansen FF, Frederickson CJ, Zimmer J, Diemer NH, 1990 Possible role of zinc in the selective degeneration of dentate hilar neurons after cerebral ischemia in the adult rat. Neuroscience letters 109, 247–252. [PubMed: 2330128]

Velasco I, Tapia R, 2000 Alterations of intracellular calcium homeostasis and mitochondrial function are involved in ruthenium red neurotoxicity in primary cortical cultures. Journal of neuroscience research 60, 543–551. [PubMed: 10797557]

Wei G, Hough CJ, Li Y, Sarvey JM, 2004 Characterization of extracellular accumulation of Zn2+ during ischemia and reperfusion of hippocampus slices in rat. Neuroscience 125, 867–877. [PubMed: 15120848]

Weiss JH, Hartley DM, Koh JY, Choi DW, 1993 AMPA receptor activation potentiates zinc neurotoxicity. Neuron 10, 43–49. [PubMed: 7678965]

Yao J, Irwin RW, Zhao L, Nilsen J, Hamilton RT, Brinton RD, 2009 Mitochondrial bioenergetic deficit precedes Alzheimer's pathology in female mouse model of Alzheimer's disease. Proc Natl Acad Sci U S A 106, 14670–14675. [PubMed: 19667196]

Yin H, Turetsky D, Choi DW, Weiss JH, 1994 Cortical neurones with Ca2+ permeable AMPA/kainate channels display distinct receptor immunoreactivity and are GABAergic. Neurobiology of disease 1, 43–49. [PubMed: 9216985]

Yin HZ, Sensi SL, Ogoshi F, Weiss JH, 2002 Blockade of Ca2+-permeable AMPA/kainate channels decreases oxygen-glucose deprivation-induced Zn2+ accumulation and neuronal loss in hippocampal pyramidal neurons. J Neurosci 22, 1273–1279. [PubMed: 11850455]

Yin HZ, Wang HL, Ji SG, Medvedeva YV, Tian G, Bazrafkan AK, Maki NZ, Akbari Y, Weiss JH, 2019 Rapid Intramitochondrial Zn2+ Accumulation in CA1 Hippocampal Pyramidal Neurons After Transient Global Ischemia: A Possible Contributor to Mitochondrial Disruption and Cell Death. Journal of neuropathology and experimental neurology 78, 655–664. [PubMed: 31150090]

Yin HZ, Weiss JH, 1995 Zn(2+) permeates Ca(2+) permeable AMPA/kainate channels and triggers selective neural injury. Neuroreport 6, 2553–2556. [PubMed: 8741761]

Highlights

- Zn^{2+} thought to enter the mitochondria via the mitochondrial Ca^{2+} uniporter (MCU)
- Mitochondrial Zn^{2+} loading and its consequences are attenuated in MCU knockout mice
- Zn^{2+} contributions to neurodegeneration are attenuated in MCU knockout
- Delayed MCU blockade attenuates mitochondrial dysfunction and neurotoxicity
- Targeting mitochondrial Zn^{2+} through the MCU may offer significant neuroprotection

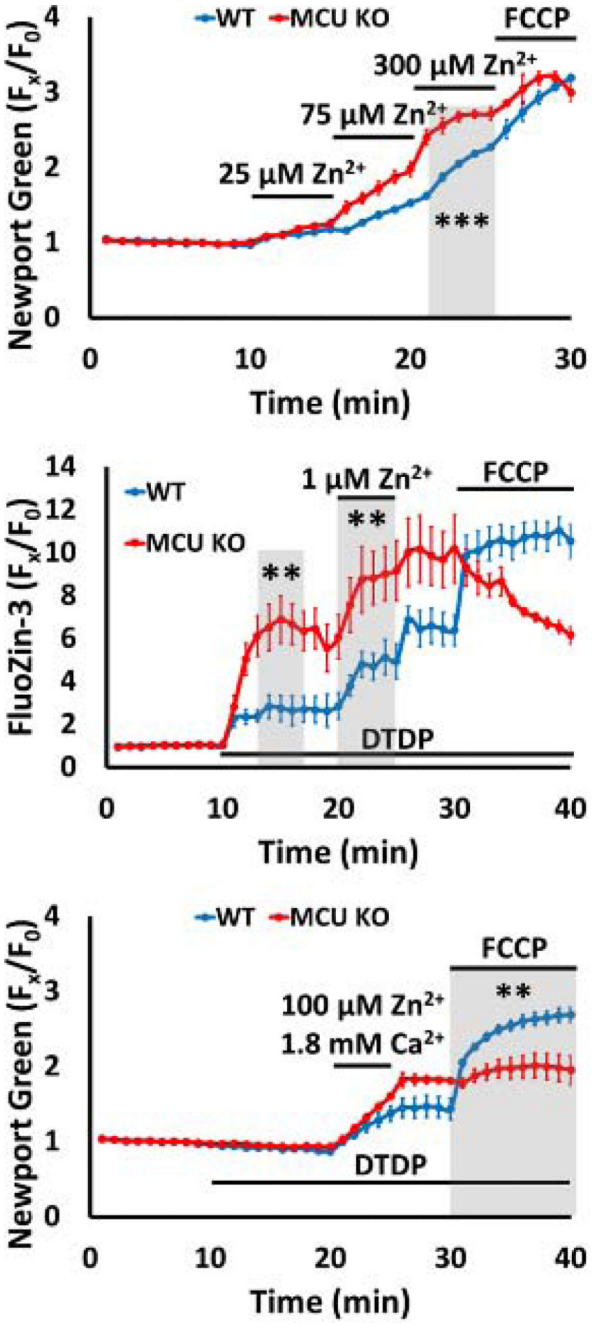

Figure 1. Mitochondrial Zn^{2+} accumulation is attenuated in mice with genetic deletion of MCU.

WT (blue) and MCU KO (red) cultured cortical neurons were loaded with either low affinity cytosolic Zn^{2+} indicator Newport Green (**top and bottom**) or high affinity cytosolic Zn^{2+} indicator FluoZin-3 (**middle**), and exposed to indicated doses of exogenous Zn^{2+} with 90 mM K^+ ("**high K^+**", along with 10 μM MK-801 to inhibit Ca^{2+}-entry through the NMDA receptor). DTDP (60 μM; to disrupt cytosolic Zn^{2+} buffering) and FCCP (1 μM; to release mitochondrially sequestered Zn^{2+}) were added as indicated. Studies were carried out in HSS with either 0 mM Ca^{2+} (**top and middle**; to ensure observations of Zn^{2+} specifically) or 1.8 mM Ca^{2+} (**bottom**; to better model physiological condition). Traces show time course of

indicator ΔF (background subtracted and normalized to baseline, [F_x/F_0]), and represent means ± standard error of the mean (**SEM**) of at least 6 experiments, consisting of ≥ 120 neurons. Grey bars indicate time points of comparison (** indicates $p < 0.01$, *** indicates $p < 0.001$, by two-tailed t-test). Note that MCU KO neurons consistently displayed greater ΔF in response to exogenous Zn^{2+} exposures and/or disrupted buffering, as well as reduced FCCP responses, both of which indicate the critical role that MCU plays in facilitating Zn^{2+} entry into mitochondria.

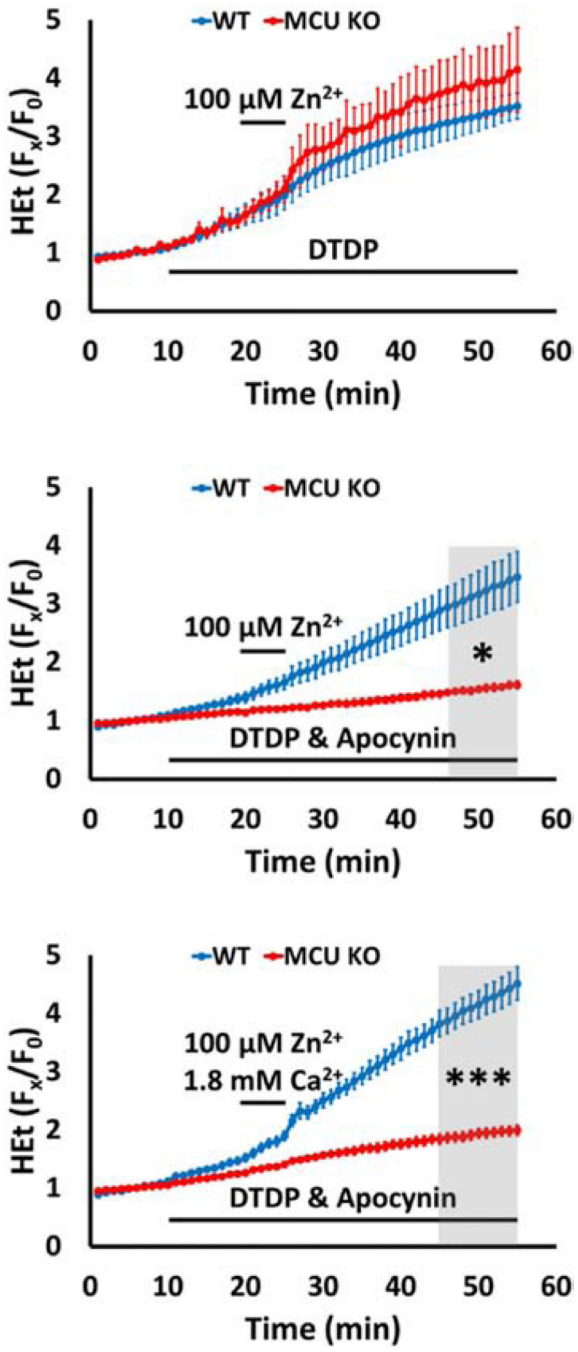

Figure 2. Zn^{2+}-triggered mitochondrial—but not cytosolic—ROS production is attenuated in MCU KO neurons.

WT (blue) and MCU KO (red) cultured neurons loaded with superoxide preferring ROS indicator Hydroethidine (**HEt**) in either 0 mM Ca^{2+} (**top and middle**) or 1.8 mM Ca^{2+} (**bottom**) HSS were exposed to 100 μM Zn^{2+} + high K^{+}, with DTDP (60 μM) and apocynin (500 μM) added as indicated. Traces display mean ± SEM F_x/F_0 values for HEt ΔF and represent ≥ 8 experiments consisting of ≥ 160 neurons. Grey bars indicate time points of comparison (* indicates $p < 0.05$, *** indicates $p < 0.001$, by two-tailed t-test). Despite the

similar total ROS generation (**top**), note that Zn^{2+}-triggered ROS rise specifically from mitochondria (assessed via addition of NOX inhibitor apocynin to attenuate cytosolic ROS production) was significantly attenuated in MCU KO neurons (**middle and bottom**).

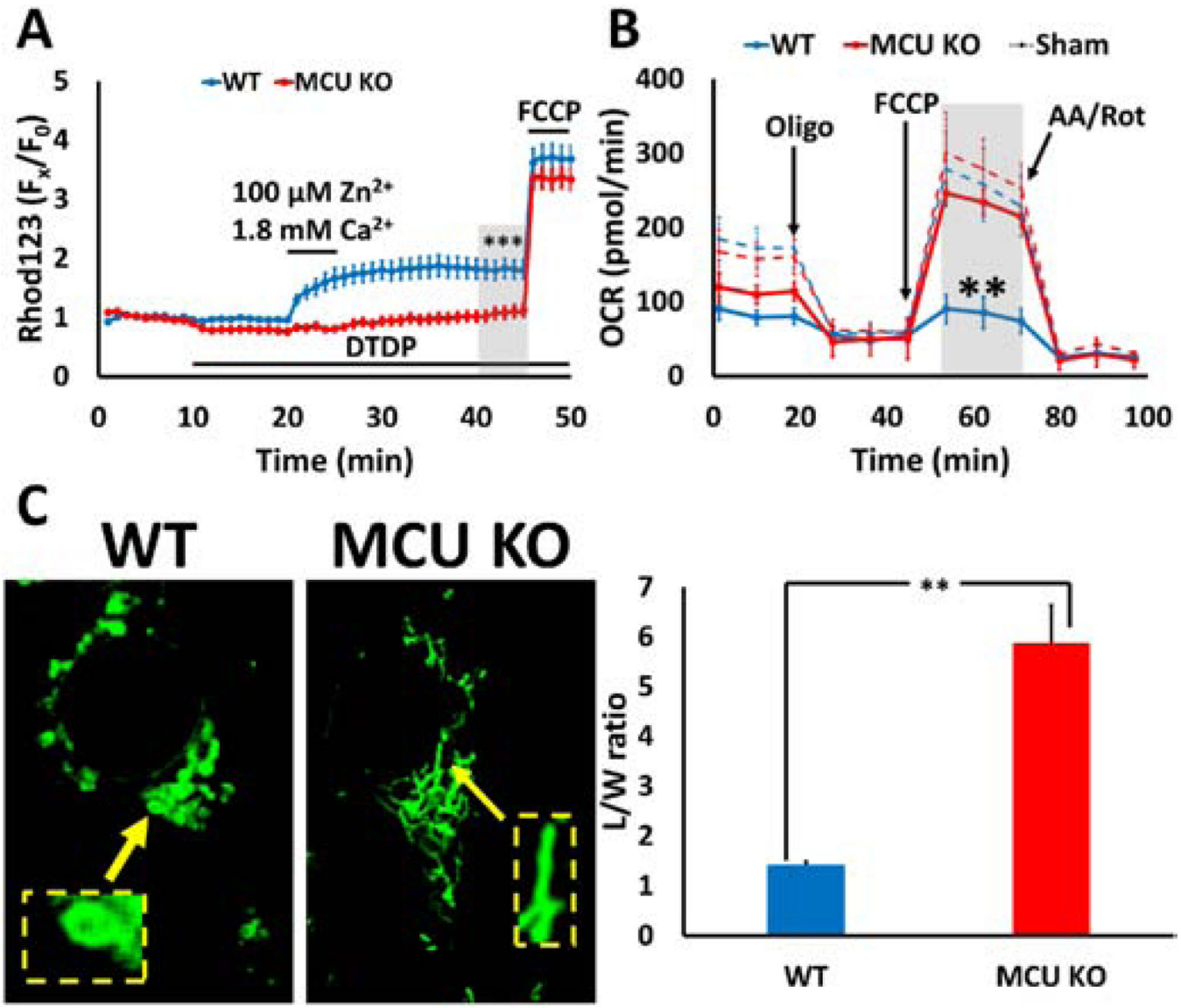

Figure 3. Genetic deletion of MCU confers prolonged protection from Zn^{2+}-triggered mitochondrial dysfunction.

WT (blue) and MCU KO (red) cultured neurons were exposed to the ischemic Zn^{2+} exposure (DTDP [60 µM; 10 min pre-exposure, followed by 5 min during Zn^{2+} exposure and 20 min during wash], 100 µM Zn^{2+} + high K^+ [5 min], followed by wash [20 min]). Grey bars indicate time points of comparison (** indicates $p < 0.01$, *** indicates $p < 0.001$, by two-tailed t-test).

A. Zn^{2+}-induced mitochondrial depolarization is attenuated in MCU KO neurons. WT and MCU KO neurons loaded with $\Delta\Psi_m$-sensitive indicator Rhodamine 123 (**Rhod123**) were treated to the ischemic Zn^{2+} exposure as indicated, followed by FCCP (1 µM; 5 min). Traces represent mean ± SEM F_x/F_0 values for Rhod123 ΔF and represent 8 experiments consisting of ≥ 160 neurons. Note the absence of Rhod123 ΔF in response to Zn^{2+} in MCU KO neurons, indicating protection from Zn^{2+}-induced mitochondrial depolarization.

B. Mitochondrial respiration is preserved after Zn^{2+} exposure in MCU KO neurons. WT and MCU KO neurons were treated to either sham (dashed lines) or the ischemic Zn^{2+} exposure (solid lines) as described above. After 2 hr incubation, cultures were placed in the Seahorse device, which measures O_2 consumption rate (**OCR**) during baseline and after sequential application of oligomycin (**Oligo**; 1 μM), FCCP (2 μM), and antimycin A/rotenone (**AA/Rot**; both 1 μM). Traces show time course of OCR and represent mean ± SEM of 3 separate experiments, each consisting of 3 – 4 wells of cultured neurons, with arrows indicating time point at which mitochondrial inhibitors were added. Note that mitochondrial respiration was preserved in MCU KO neurons in response to Zn^{2+}, compared to its dramatic inhibition WT.

C. MCU KO neurons are protected from Zn^{2+}-triggered disruption of mitochondrial morphology. 12 hrs after WT and MCU KO neurons were treated to ischemic Zn^{2+} exposure, mitochondria were labeled with MitoTracker Green and observed under confocal microscopy (1000x). Length/width ratio (**"L/W ratio"**) was calculated based on blinded measurement. Representative images (**left**) and average L/W ratios (**right**) for WT and MCU KO neurons are displayed. Bar graphs show mean + SEM of L/W ratio, each representing ≥ 5 experiments comprising ≥ 50 mitochondria. Note the significant mitochondrial fragmentation and swelling in WT neurons, compared to the elongated morphology maintained by MCU KO neuronal mitochondria, both of which correspond to their respective L/W ratios.

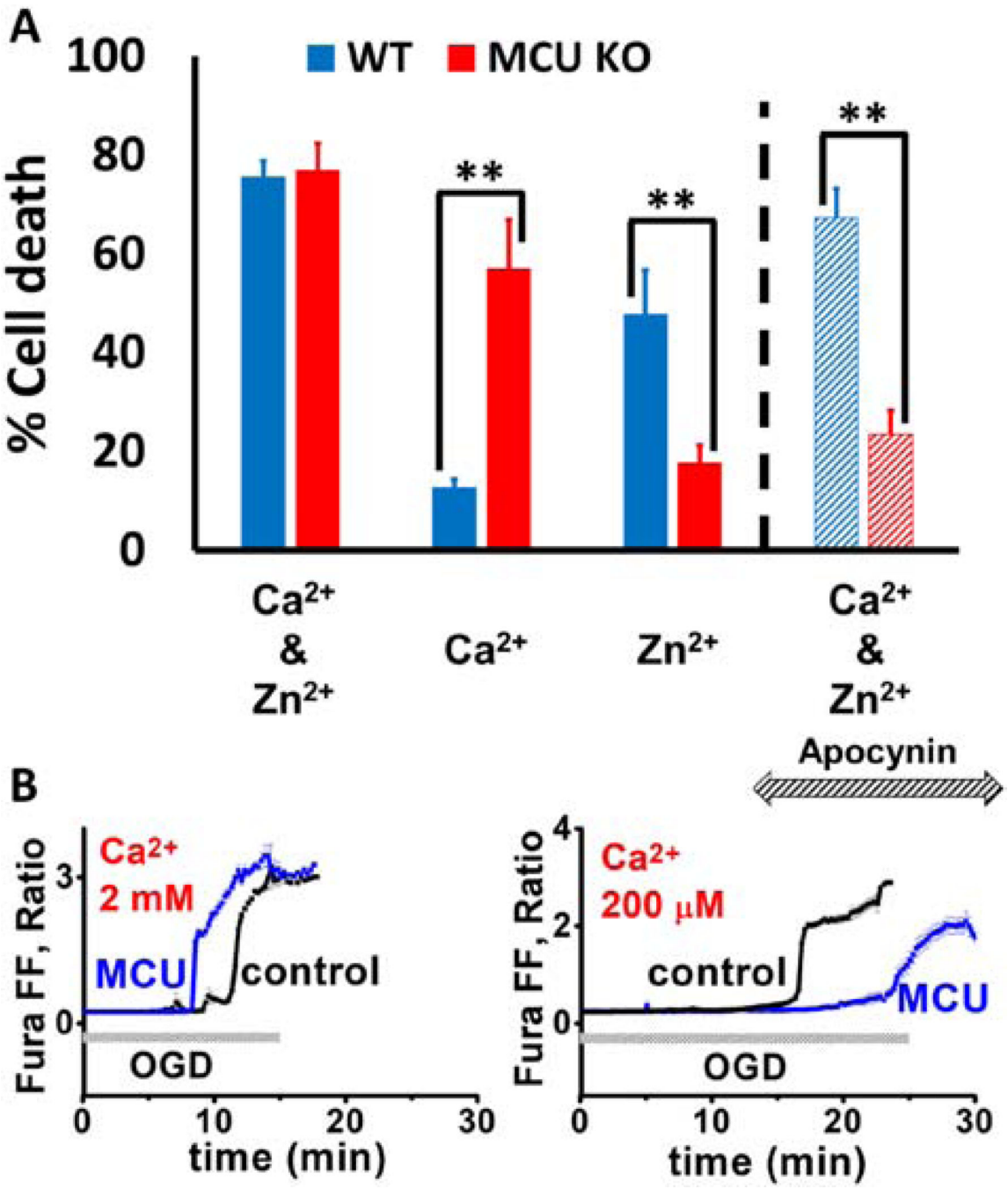

Figure 4. Zn^{2+}-specific contributions to neurotoxicity and ischemic neurodegeneration are attenuated in MCU KO cultured neurons and hippocampal slices.

A. Zn^{2+}-triggered neurotoxicity is attenuated in cultured MCU KO neurons. WT (blue) and MCU KO (red) neurons were treated to the following exposures: "**Ca^{2+} & Zn^{2+}**" (10 min pre-exposure to 60 μM DTDP, followed by 5 min 100 μM Zn^{2+} + high K^+ + MK-801 + DTDP and 3x wash into DTDP for 20 min, all in 1.8 mM Ca^{2+} HSS), "**Ca^{2+}**" (5 min exposure to high K^+ + MK-801, followed by 3x wash for 20 min, all in 1.8 mM Ca^{2+} HSS), "**Zn^{2+}**" (same as "Ca^{2+} & Zn^{2+}" except in 0 mM Ca^{2+} HSS), or "Ca^{2+} & Zn^{2+}" with

Apocynin (same as "Ca^{2+} & Zn^{2+}" with 500 μM Apocynin co-present with DTDP; indicated by diagonal striped bar). After 24 hr incubation, cell death was quantified with LDH efflux assay and validated with direct morphological examination. Concentrations used are indicated. Bars represent mean % cell death ± SEM of 6 independent experiments, each consisting of 4 wells of cultured neurons. Note that MCU KO neurons showed heightened sensitivity to Ca^{2+} triggered injury, but with attenuation of the Ca^{2+}-contributions (either via Ca^{2+}-free conditions or NOX inhibition with apocynin), MCU KO neurons were significantly protected from Zn^{2+}-triggered neurotoxicity.

B. Ischemic neurodegeneration is delayed in MCU KO hippocampal CA1 neurons when Ca^{2+}-contributions are moderated. Individual CA1 pyramidal neurons in hippocampal slices from WT (black; "**control**") or MCU KO (blue; "**MCU**") were loaded with the cytosolic Ca^{2+} indicator Fura FF and subjected to prolonged OGD in ACSF containing either 2 mM (**left**) or 200 μM (**right**) Ca^{2+}. Traces show time course of ratio of Fura FF emissions upon excitation at 340 and 380 nm and represent mean ± SEM of ≥ 5 separate repetitions. Note that while MCU KO CA1 neurons showed more rapid Ca^{2+} deregulation (as indicated by irreversible Fura FF signal rise) with physiologic (2 mM) Ca^{2+} (**left**; likely due to rapid, unbuffered cytosolic Ca^{2+} accumulation leading to more rapid catastrophic injury), when effects of Ca^{2+} were attenuated, ischemic neurodegeneration was significantly delayed (**right**).

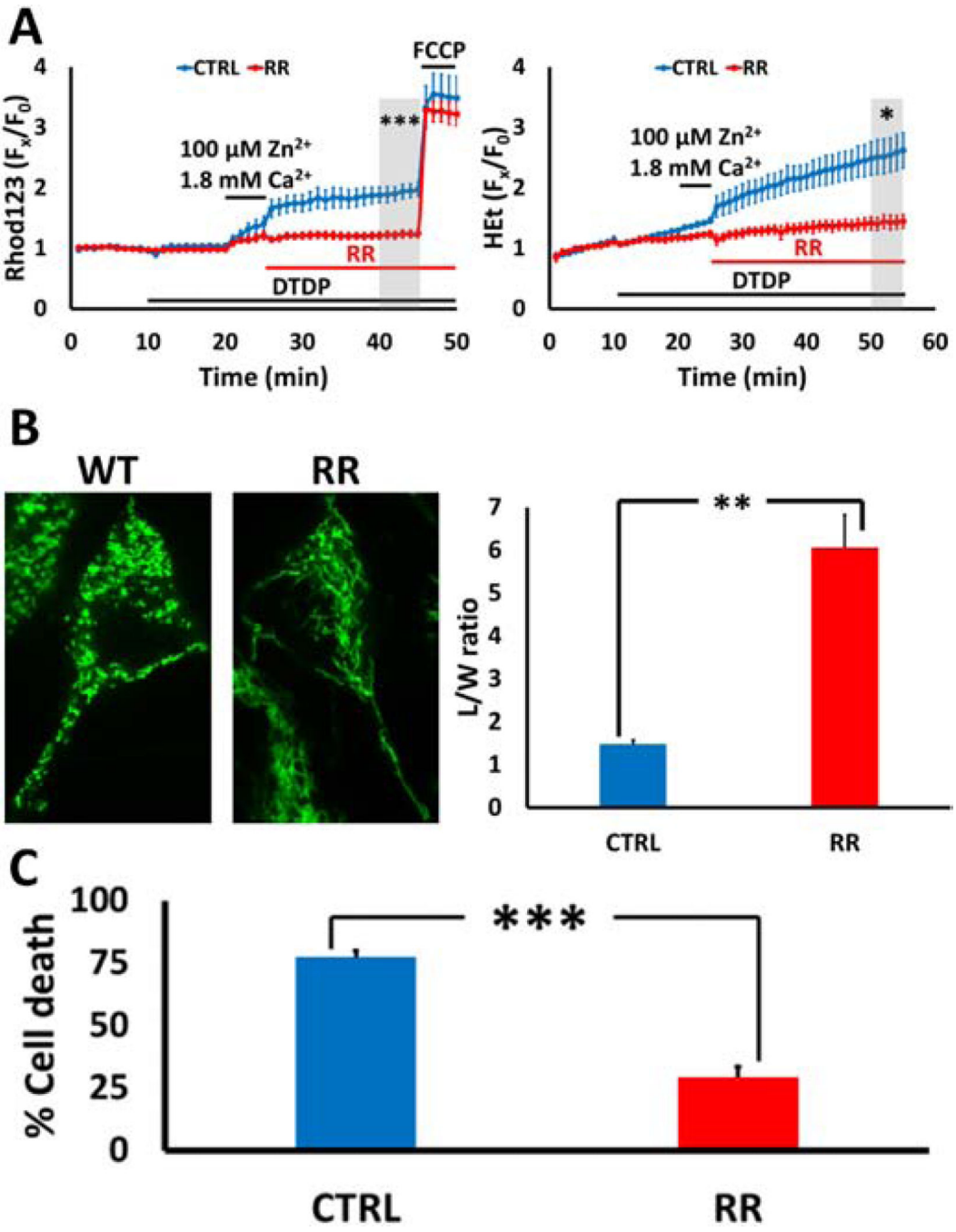

Figure 5. Delayed MCU blockade attenuates the Zn^{2+}-triggered mitochondrial dysfunction and neurodegeneration.

WT neurons were exposed to the ischemic Zn^{2+} exposure, followed by 20 min wash into DTDP alone (blue, "**CTRL**") or DTDP + 10 µM RR (red, "**RR**"). Traces represent mean ± SEM F_x/F_0 values for indicator ΔF (**A**) and represent 8 experiments consisting of ≥ 160 neurons. Bar graphs show mean + SEM of either L/W ratio (**B**) or % cell death (**C**), each representing ≥ 5 independent experiments. Grey bars indicate time points of comparison (** indicates $p < 0.01$, *** indicates $p < 0.001$, by two-tailed t-test).

A. Delayed MCU blockade attenuates acute Zn^{2+}-triggered mitochondrial dysfunction. Neurons loaded with either Rhod123 (**left**) or HEt (**right**) were treated to the ischemic Zn^{2+} exposure as described above, with FCCP (1 μM) added in Rhod123 loaded neurons as indicated. Note that delayed RR attenuated both loss of $\Delta\Psi_m$ (**left**) and rise in ROS production (**right**) in response to Zn^{2+} exposure.

B. MCU blockade after Zn^{2+} exposure preserves mitochondrial morphology. WT neurons were treated to the ischemic Zn^{2+} exposure as described above. After 12 hr incubation, neuronal mitochondria were labeled with MitoTracker Green and observed under confocal microscopy (1000x), after which L/W ratio of mitochondria were calculated blindly. Note the preserved mitochondrial structure (indicated by their elongated morphology [**left**] and corroborated with high L/W ratio [**right**]) in RR-treated neurons.

C. Delayed MCU blockade attenuates neurodegeneration. WT neurons were treated to the ischemic Zn^{2+} exposure as described above. After 24 hr incubation, cell death was assessed via LDH efflux assay. Note that delayed MCU blockade (via transient RR treatment) significantly attenuated Zn^{2+}-triggered neurotoxicity.